CHALMERS
UNIVERSITY OF TECHNOLOGY

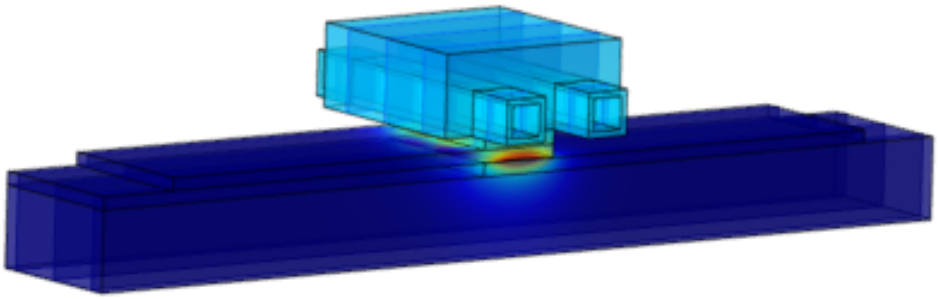

Simulation of induction welding process for glass fiber thermoplastic composites in aerospace applications

Master's thesis in Mechanical Engineering

Allen Jahromi

Department of Industrial and Materials Science
CHALMERS UNIVERSITY OF TECHNOLOGY
Gothenburg, Sweden 2019

MASTER'S THESIS IN MECHANICAL ENGINEERING
2019

Simulation of induction welding process for glass fiber thermoplastic composites in aerospace applications

ALLEN JAHROMI

CHALMERS
UNIVERSITY OF TECHNOLOGY

Department of Industrial and Materials Science
Division of Material and Computational Mechanics
Chalmers University of Technology
Gothenburg, Sweden 2019

Simulation of induction welding process for glass fiber thermoplastic composites in aerospace applications
Allen Jahromi

© ALLEN JAHROMI, 2019.

Supervisor: Professor Yuriy Serdyuk, Department of Electrical Engineering, Chalmers University of Technology.
Supervisor: Professor Martine Dube, École de technologie supérieure ÉTS, Department of Mechanical Engineering.
Supervisor: Dr. Mohammad Rouhi, Structural Analysis & Modeling Group RISE SICOMP AB.

Examiner: Associate professor Martin Fagerström, Department of Industrial and Materials Science, Chalmers University of Technology.

Master's Thesis 2019: Mechanical Engineering
Department of Industrial and Materials Science
Division of Materials and Computational Mechanics
Chalmers University of Technology
SE-412 96 Gothenburg
Telephone +46 31 772 1000

Cover: Simulation of induction welding process for glass fiber thermo-plastic composites in aerospace applications.

Typeset in LaTeX
Printed by Chalmers Reproservice
Gothenburg, Sweden 2019

Simulation of induction welding process for glass fiber thermoplastic composites in aerospace applications

Allen Jahromi
Department of Industrial and Material science
Division of Material Computational Mechanics
Chalmers University of Technology

Abstract

The use of high-performance thermoplastic composite material has increased. It is therefore relevant to study in depth their joining processes and to determine the joining parameters allowing for good mechanical performance. The current study focuses on the induction welding technology as one of the most promising method for this purpose. To understand physical background of inductive welding of thermoplastic composites and to propose methods for optimizing the process, a three dimensional finite element model of the induction heating process for induction welding of glass fiber polyetherimide (GF/PEI) is developed using the COMSOL Multiphysics® software. The model takes into account a stainless steel mesh net susceptor placed at the welding interface of the two adherends to be welded. The eddy-currents in the susceptor being generated by time-varying external magnetic field, provide heat at the welding interface, where it is needed. The model predicts the temperature rise within the material during the heating of welding process. Also, a sensitivity analysis is performed aiming at identifying the parameters and properties that have the greatest effect on temperature. These are input current, frequency, distance between coil and susceptor and electrical conductivity of the susceptor.

Keywords: Thermoplastic Composites, Induction Welding, Fusion bonding, Finite Element method, Aerospace Application, Controlling edge effect.

Acknowledgements

I would like to express my sincere gratitude to professor Martine Dube for her advice and providing the opportunity to conduct my experiments at composite laboratory at École de technologie supérieure (ÉTS). My special thank goes to professor Yuriy Serdyuk for bringing a great competence in electrodynamics to this project and valuable advise for making a simulation model. I would also like to express my profound gratitude to professor Martin Fagerström and Dr.Mohammad Rouhi for their great support throughout this work.

I would like to also acknowledge researchers at RISE SICOMP AB, particularly Robin Olsson and Erik Marklund for their valuable guidance throughout this project.

Allen Jahromi, Gothenburg, June 2019

Contents

1
Introduction

Structural parts and assemblies made of fiber reinforced thermoplastic composites are being developed to be included in current aeronautic structures. Thermoplastic composite technology intends to achieve improved properties and low-cost processes [1, 2]. Fiber glass thermoplastics are known to have high melting temperature as well as high impact resistance, where these characteristics justify the fact to utilize fiber glass thermoplastics for manufacturing parts such as nose-cone and leading edges on wings for aircraft industry. Induction welding of different thermoplastic composite parts permits to obtain assemblies with lower weight and cost saving benefits.

Currently, joining of composite materials is a matter of intense research [3], since traditional joining technologies such as riveting are not directly transferable to thermoplastic composite structures [3, 4]. Conventional joining methods, for example, use of rivets result in stress concentrations and delamination [5]. Therefore, over the past few years, new methodologies have been developed [6]. Since limitations such as lack of large hot press mold do not allow to manufacture components in a single step, the need for a reliable assembly method has emerged significantly. Traditional mechanical fastening methods such as fasteners and rivetting increase weight, rise stress concentrations around joints and cause delamination due to drilling [7]. Also use of mechanical fasteners with different thermal expansion coefficient results in induced stress. On the other hand the cost of titanium fasteners is another disadvantage to consider fusion bonding as an effective method for joining different components. Using thermoplastics comes with the advantage of high fracture toughness and damage tolerance, also due to the ability to form thermoplastics with low cycle time and manufacturing cost, it has drawn attentions for a suitable method for fusion bonding for assembling thermoplastic components [8]. Fusion bonding technology, which originated from the thermoplastic polymer industry, has gained a new interest with the introduction of thermoplastic matrix composites. The use of thermoplastic resin as hot melt adhesives is an alternative to mechanical fastening and thermosetting adhesive bonding.

There are different methods for fusion bonding such as ultrasonic welding and resistance welding of thermoplastic composites [9], however induction welding is to be the focus of this study. Induction welding of thermoplastic composites is a non-contact welding method in which two piece-works are welded together using a conductive and/or magnetic thin heating element at the welding interface. Due to magnetic susceptibility of the heating element from now on we call it susceptor. When the susceptor is exposed to alternating magnetic field generated by a coil, joule and

hysteresis loss in the susceptor generates heat at the weld interface. This heat melts the polymer matrix at the welding interface and results in welding. Figure 1.1 illustrates a single lap-shear configuration of induction welding.

When considering manufacturing process, it is important to determine the values of the processing parameters to have successful processing. Process modeling is very important because it facilitates the optimization of the processing parameters and helps to avoid expensive and lenghtly experimental testings. In fusion bonding process modeling is mainly consist of electromagnetic problem, heat transfer and consolidation. Other aspects influencing the final strength of the joint such as crystallization are out of scope of this work. The objective of heat transfer modeling is to predict temperature at welding interface.

1.1 Induction Welding

Induction welding includes several steps: 1) surface preparation, 2) heating, 3) pressing, 4) intermolecular diffusion and 5) cooling. For induction welding there is need for a heat source as a heating element at the welding interface. This heating element is called susceptor. For this purpose a stainless steel net mesh is used as a susceptor at the welding interface. As glass fiber thermoplastics are electrically non-conductive and also non-magnetic, the heat generation process will be just within the stainless steel susceptor by the joule effect and hysteresis effect. Figure 1.1 demonstrate lap-shear set up in induction welding process, where you can see different active parts [8].

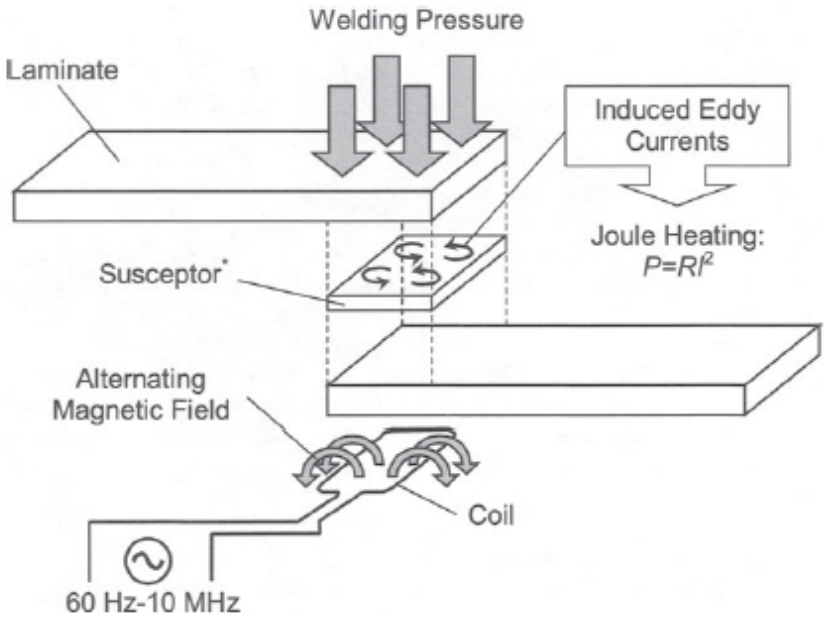

Figure 1.1: Induction welding set-up [8]

1.1.1 Surface Preparation

Welding of thermoplastic composites has shown tolerance towards contamination at the welding zone. Compared to thermoset adhesives, in the welding of thermoplastic composites the surface preparation is less critical. Experiments with release agents showed that small amounts of silicone contamination did not affect the quality of the weld [1]. However having smooth surfaces is crucial for homogeneous heat transfer at the welding interface. Accordingly, the surface preparation is usually the first step in composites welding and often involves machining or cleaning [2]. Machining is necessary for intimate contact, also to ensure geometrical fit of the parts to be welded, this is very important as ensures proper contact between components in which leads to desired heat transfer between them [2].

1.1.2 Heating

Induction heating is a non-contact heating process used for heating electrically conductive materials. When such conductive materials are exposed to an alternative magnetic field, local eddy-currents will be induced on the surface of material. There is a depth associated to this surface in which eddy-currents exist and it is called skin-depth. These eddy-currents generate heat due to joule losses. Joule losses as explained in Figure 1.2 is the only mechanism in which generates heat in a stainless steel susceptor. Heating mechanism is different [10] when laminates contain conductive and/or magnetic components. For example, in a conventional quasi-isotropic carbon fiber thermoplastic composite, because the carbon fiber itself is conductive so it will also contribute as heating source in addition to the susceptor.

There are two mechanisms in which fibers generate heat and that relays on how fibers make closed loop in cross-plies to host local eddy-currents: 1) Fiber heating by joule losses and 2) Junction heating at the fiber junction which divides into contact resistance heating and dielectric heating. Figure 1.2 demonstrates these heating mechanisms [10].

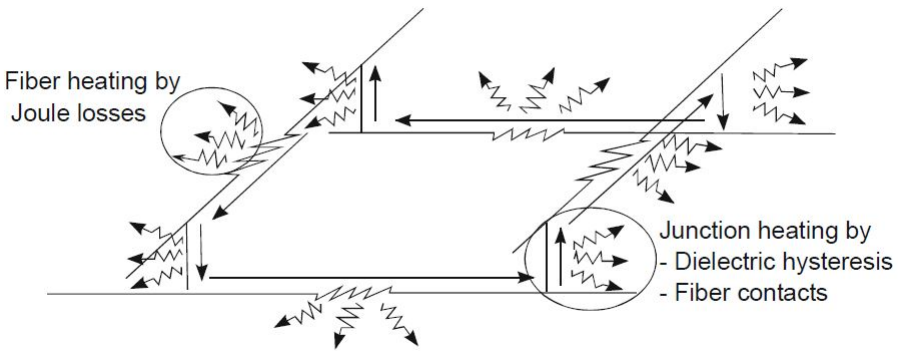

Figure 1.2: Induction heating mechanisms for fiber reinforced polymer composites [10]

1.1.3 Pressing

After heating of the welding interface, intimate contact must be established between the laminates to be welded. The contact area is reduced in the existence of imperfections at the contacting surfaces. In order to improve mechanical performance of the welding, it is therefore important to increase the contact area at the welding interface, by applying pressure [2]. As soon as pressure is applied, consolidation will be initiated due to the heat transfer.

Figure 1.3, demonstrates the time to achieve intimate contact versus consolidation pressure [2]. Pressing can be divided into two phases: 1) Surface roughness are removed and intimate contact is developed. 2) Molten matrix is squeezed out, displacing trapped gases in the welding interface. It is crucial that polymer squeeze-out occurs at the welding interface as quick as possible during the welding process [2], because having gases/small bubbles at the weld zone cause stress concentrations. Accordingly, achieving a low viscosity condition is very crucial. This is more important for composites with high fiber volume contents and highlights the importance of the heating step, because viscosity is temperature-dependent. In order to improve polymer-polymer bond it is beneficial to apply a thermoplastic resin film at the welding interface. The reason is the squeeze-out of the resin can be achieved easier than composites [1].

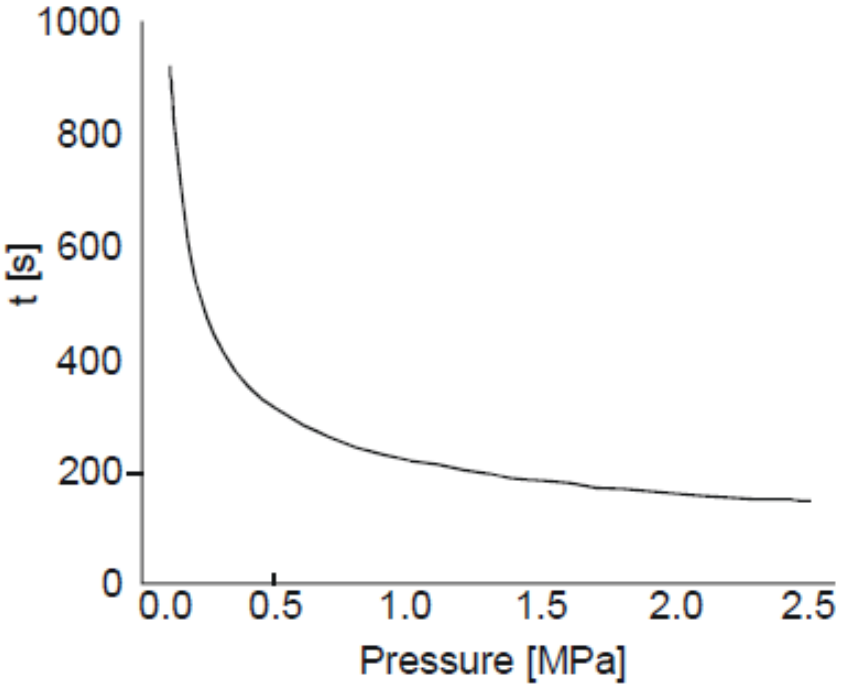

Figure 1.3: Two surface in contact [11]

1.1.4 Intermolecular Diffusion

After performing intimate contact at the interface, intermolecular diffusion and mix-up of polymer chains is necessary to initiate the welding at the interface [2]. The interface slowly disappears and the mechanical strength at the polymer interface initiates. This process is referred to as autohesion. This can be divided into five different phases [12]: 1) Surface rearrangement, 2) surface approach, 3) wetting, 4) diffusion, 5) randomization. In welding, the first three phases are part of the pressing step whereas phases 4 and 5 are parts of the diffusion step [2]. Under ideal conditions, the interface is not noticeable from the bulk at the end of the process. For amorphous thermoplastic polymers, intermolecular diffusion is possible at temperatures above T_g [2]. For semi-crystalline polymers, melting temperature T_m has to be exceeded. Below melting temperature welding can not be achieved, because crystallites bind the molecules, while above T_m, intermolecular diffusion is very rapid [2], [13].

1.1.5 Cooling

Cooling is the last step in induction welding and at this step consolidation of the material occurs. Semi-crystalline materials will re-crystallize and amorphous polymers retain the molecular orientation obtained previously [14]. The cooling rate determines the crystallinity and the formation of spherulites in the welding interface [2]. This will also determine mechanical properties of the weld.

1.2 Induction Heating Process

It was previously explained, heat is produced in conductive or magnetic material as a response of these materials to the alternating current (AC) magnetic field. For this study glass fiber Polyetherimide (PEI) is used, because glass fiber is not conductive nor magnetic, so heat generation process is dominated by stainless steel mesh net susceptor through joule loss and small contribution of hysteresis loss.

Manufacturing and plastic deformation of the steel mesh susceptor results in change in magnetic properties of the susceptor, this leads to a small contribution of hysteresis loss [15, 16]. Since the contribution of hysteresis loss is small, it is neglected in this study.

Joule loss: wires in a metal mesh generates heat due to the inherent resistance of the wires and is therefore dependent on wire's length, resistivity, and cross sectional area.

Hysteresis loss:heating process also occurs due to hysteresis losses in ferromagnetic materials. When these materials are exposed to an alternating magnetic field these material will heat up [16]. Hysteresis indicates the energy which is needed to turn around the small internal magnets of the material to align with the alternating magnetic field. As it is illustrated in Figure 1.4, rotation of magnetic dipoles causes friction and vibration, this energy is lost in the form of heat [16].

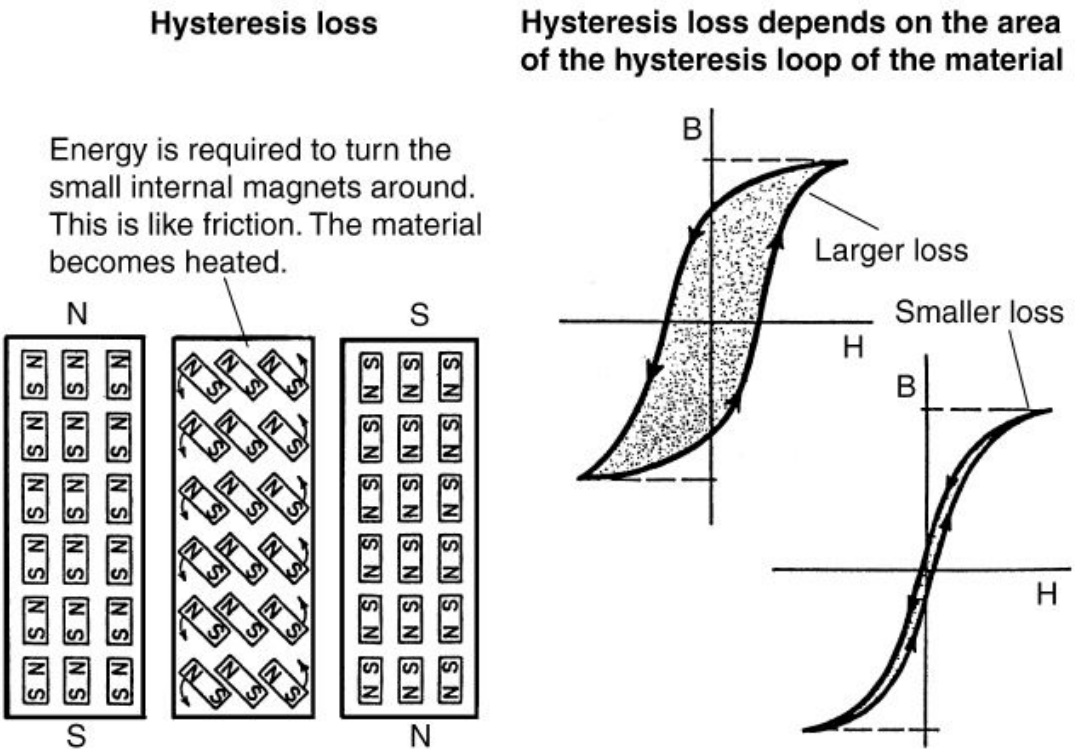

Figure 1.4: Effect of hysteresis on heating rate. N, north; S, south; B, flux density in a ferromagnetic material; H, corresponding magnetic intensity [16].

1.3 Susceptor (heating element)

In cases where adherends are not conductive nor magnetically susceptible, heating elements are used to provide localized heating at the weld zone. There are several type of heating element for induction welding. They come in the form of powder or mesh [17]. The requirement for using materials as a heating element is that they are susceptible to the electromagnetic field and have enough electric resistance to develop heat and form a conductive close-loop to host the local eddy-currents. The use of magnetic/conductive heating elements have advantages even when the adherends is carbon fiber reinforced. First and foremost, heat can be generated exactly where it is necessary at the welding interface, so it prevents thermal stress development in the work-piece. The susceptor can be also coated with resin to help blending two matrices.

1.4 Edge Effect in Susceptor

One of the major issues associated with induction welding is an effect arising from the geometry of the weld zone. This so-called "edge-effect" results from a coil's proximity to an edge of the susceptor. As an example, if a simple circular pancake coil is considered, eddy currents induced in the susceptor create global current loops that

are circular. Figure 1.5 (i) shows the eddy current path produced by such a coil and an example of the corresponding temperature profile taken across line A–A, for a susceptor that is larger than the coil. At the edges, and especially at the corners, there is a large area for eddy currents to flow [17]. This results in lower current densities in these regions and less heat is generated, as shown by the lower temperature profiles at the edges of the susceptor. If the size of the susceptor is reduced, as shown in Figure 7 (ii) and (iii), the eddy-currents are unable to follow the shape of the coil. In order to create closed-loop paths, the eddy currents are then forced to travel along the edge of the laminate in closest proximity to the coil [17]. As a result higher current densities and higher temperatures in these regions occur, as indicated by the temperature profiles.

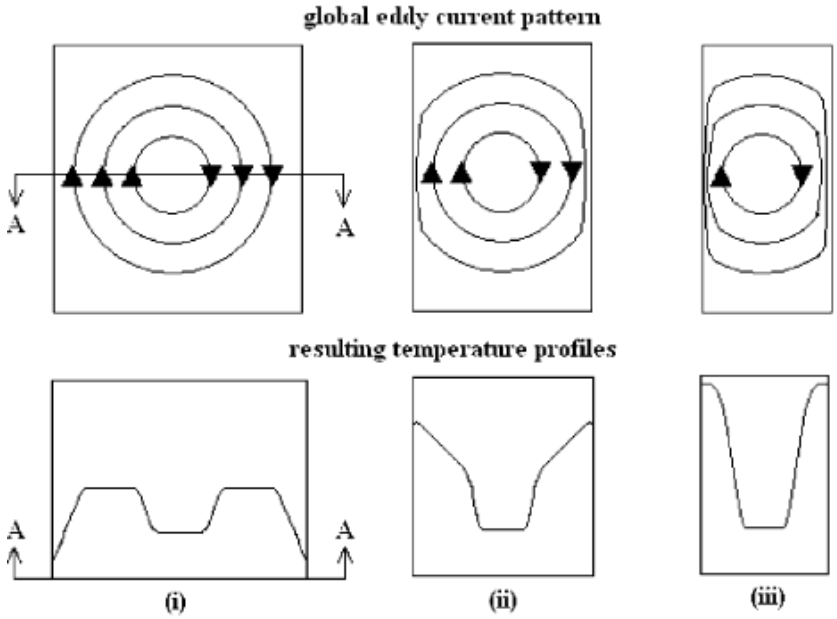

Figure 1.5: Edge-effect [17]

It is the higher temperatures that arise at the edge of the susceptor that is the most difficult to eliminate and there have been some efforts to minimize edge effects, or to avoid them altogether. The simplest and most common method is to use models to predict where excessive edge heating may occur. Changes to the coil design can then be made to counteract this effect [18]. However, the procedure becomes more complex as the coil design, susceptor geometry and layup becomes more complex. Another method was chosen to prevent edge effects by modifying the susceptor. The process involves redirecting eddy current flow paths in metal mesh susceptors by selectively cutting patterns in the mesh. Once again, models can be used to predict heat generation for a given mesh configuration at first, then optimizing cut patterns to create more uniform heating in areas where overheating may occur [19]. Along similar lines, mesh susceptors with solid foil edges, i.e. edges with zero mesh opening, can also work to reduce the effect of edge effect. In this way, wherever the current density is higher, the resistance is lower and therefore the temperature can

be reduced [20]. Figure 1.5 illustrates the edge effect. Such high induced current density on the edge can cause temperature gradients and thermal degradation.

1.5 Skin Effect in Susceptor

When a direct current (DC) flows through an electrically conductive material, the current distribution over a cross sectional area of such a conductive material is uniform. On the contrary when alternating current (AC) is applied to the same material the distribution will become non-uniform [17]. This is due to the fact that such induced current by an AC source tends to flow outwards at the surface of the material instead of penetrating the cross-section with the same density as the current develops on the surface of the material. The result of such a phenomena (skin effect) is that most of the heat is developed on the surface of the material. Figure 1.6 demonstrates the skin-effect [17].

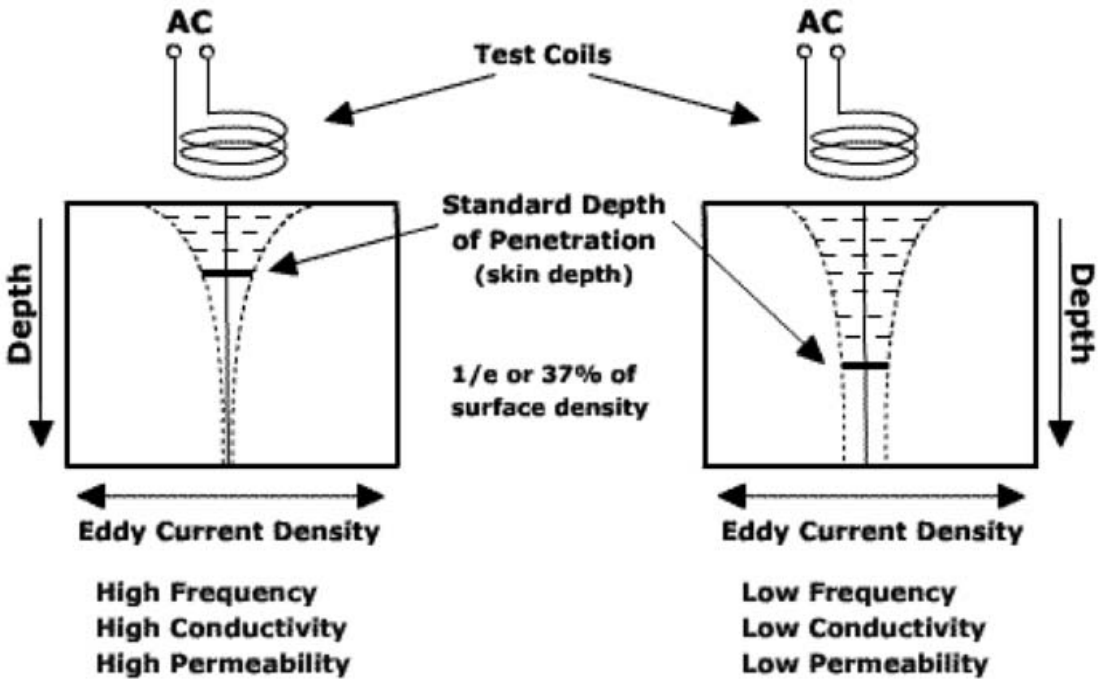

Figure 1.6: Skin-effect [17]

In order to predict values for skin effect, the reference depth is used and defined as the depth in which the eddy current density has reduced. The reference depth depends on material property such as electrical resistivity, magnetic permeability and the frequency of the coil. Skin-depth is estimated by the equation below [17].

$$\delta = \sqrt{\frac{2\rho}{\mu\omega}} \tag{1.1}$$

where $\rho[\Omega m]$ is resistivity of the susceptor, $\omega[Hz]$ is the angular frequency of the coil and $\mu[H/m]$ is the electric permeabity. As Equation 1.1 is showing, by increasing the frequency of the coil the reference depth decreases and thus a more shallow skin effect is expected. Figure 1.6 demonstrates how variables shown in Equation 1.1 effects the penetration depth.

1.6 Proximity Effect

The proximity effect happens between the current in the induction coil and the induced eddy-current in the susceptor. Accordingly most of the current in the coil is forced to flow along the surface of the coil which is closest to the susceptor. The induced eddy-currents in the susceptor is in the opposite direction with respect to the current on the surface of the coil. This is an advantageous effect because currents are attracted to each other. In order to increase the proximity effect between the induction coil and the susceptor a C-shape flux concentrator can be placed on top of the coil.

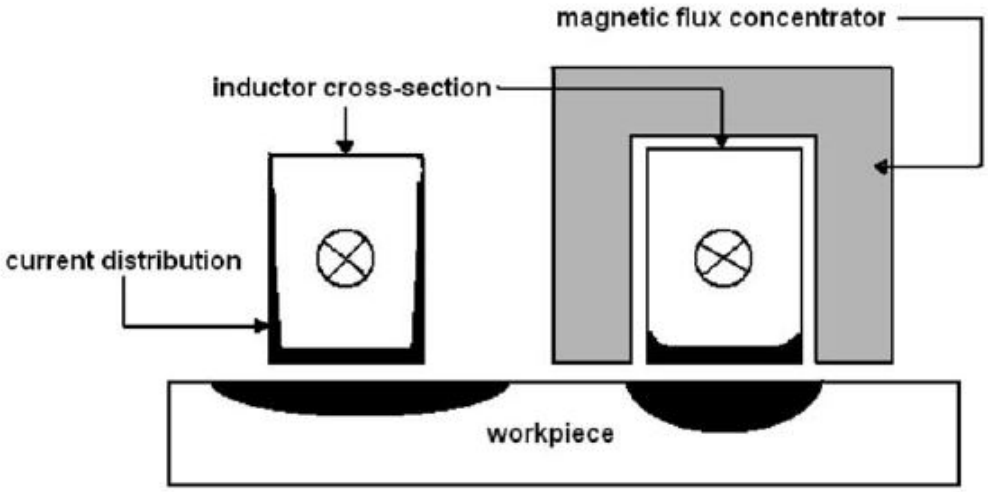

Figure 1.7: Magnetic flux concentrator [17]

A flux concentrator is a magnetically conductive material which is able to provide an easier path to transit and conduct the magnetic field more efficiently and effectively than air. Three groups of materials may be used for flux concentrators; laminates of silicon steel, ferrites and magneto dielectric materials. Flux concentrators direct, focus and control magnetic fields into a specific area of the coil while isolates the

areas around the coil which does not need to generate heat. In other word, it increases the ability to enforce localized heat generation. Figure 1.7 demonstrates a flux concentrator and its functionality [17].

1.7 Induction Welding Parameters

1.7.1 Machine parameters

Frequency:
The current frequency is an important parameter, because eddy currents are induced due to the alternating magnetic field. Experiments show that for higher frequencies the heating rate increases [21].

Power/Current:
According to Haimbaugh et. al [16] the power output is one of the most important parameters of induction heating process. This is discussed further in sensitivity studies.

Coupling distance:
When the coupling distance between the coil and the work-piece is increased the magnetic field intensity drops. This drop is proportional to $\frac{1}{d^2}$, where d is the coupling distance between coil and work piece. According to Ageorges et. al [8] the magnetic field of the coil $H(A/m)$ is calculated by Equation 1.2 as follow.

$$H = \frac{I}{4\pi} \int_0^L \frac{r \; dl}{|r^3|} \tag{1.2}$$

where dl is an element of the current carrying conductor and r is the position vector between the element dl and the point P where the magnetic field H is measured. Current intensity in the coil is $I[A]$ and $L[m]$ is the length of coil.

1.7.2 Material Parameters

Apart from machine parameters discussed in the previous subsection, there are several material parameters to be used as the input for the induction heating model. Because material properties such as resistivity are temperature dependent, it is difficult to measure these parameters and reliable data are not always accessible. Among several properties to be used, the following material parameters are considered as most important

Electromagnetic Material Properties:
The electromagnetic properties that are used for quasi-static modeling of induction heating are:

- Electrical conductivity σ

- Relative permeability μ_r
- Relative permittivity ϵ

Thermal Material Properties
The following properties are used for thermal modeling of the heating step:

- Density ρ
- Heat capacity C_p
- Thermal conductivity k_T

The density is assumed to be constant in the temperature range under analysis in the model.

1.8 Pressure

Application of appropriate pressure is crucial for high quality consolidation [22]. However, it has been realized there is a limit to the pressure that can be applied. This is because applying high pressure can results in excessive squeeze-out of matrix, which can lead to low quality weld. So an optimization needs to be done between adequate intimate contact and polymer squeeze-out. Poor pressure application can result in the following faults:

1. Voids: appearance of voids have close relationship to deconsolidation of the polymer. Heat expansion of small air packets trapped in the welding interface can result in voids at the welding interface. To avoid voids it is important to consider high surface smoothness and then apply sufficient pressure to suppress the occurrence of voids. In some cases delamination is due to large air pockets remaining in the welding interface and matrix. These pockets later on will separate layers in the laminate and thus disrupt interaction between layers.

2. Cracks: it was reported that cracks occur due to thermal stresses by thermal expansion mismatch between fiber and the matrix. It is possible to prevent cracks by applying right amount of pressure during cooling phase. Thus the matrix is prevented from expansion and shrinkage. Pressure must be removed when we have a uniform temperature profile and when the temperature is well below melt of glass transition.

3. Folds and flashes: these defects are due to misalignment as well as poor application of pressure. In the case when the pressure is unevenly applied to the welding area, it can result in matrix flow-out causing flashes, or it can result in folding of the laminate at the edge of the pressure device and causes fibers to buckle. To prevent flashes it is important not to apply too much high pressure and in order to avoid folds it is crucial to maintain very smooth surfaces.

Residence time: residence time is the time in which the laminate is exposed to AC

magnetic fields and affect the movement of polymer molecules across the welding interface. If the machine welding parameters, frequency, power and pressure are considered to be constant, then three welding regimes can be expected related to the residence time and achieved final temperature for that duration; 1) non-wetting, 2) uniform fusion and 3) thermal degradation. Inadequate weld time does not allow matrix to melt sufficiently thus the weld strength is poor. A period of uniform fusion is described as for the residence time in which results in high quality weld, where residence time allows the material to reach glass temperature T_g, and exceed it for movement of polymer molecules in the welding interface. This is the optimized regime for residence time to achieve high quality weld. Finally, if temperature during the residence time exceeds thermal degradation will occur and consequently results in a low weld quality.

1.9 Innovation in induction welding

Most research in induction welding of thermoplastics is on developing fast and efficient heat generation process. One of the concerns in induction welding of carbon fiber reinforced thermoplastics is the risk of current leakage from welding interface to other layers. This is due to the fact that carbon fibers are conductive. This results in bulk heating of laminate and does not allow concentrated localized heating. In a study done by Worrall et. al [23], layers of electrically insulating films are used to avoid current leakage into other layers, so the heat generation is focused at the welding interface. Figure 1.8 demonstrates this study [23].

In another work done by Farahani et. al [24], carbon nano fibers (CNFs) coated with silver and nickel were manufactured as a conductive film to be used as susceptor. Using this susceptor results in higher heating rate, also provides higher lap shear strength. Figure 1.9 demonstrates this type of susceptor [24].

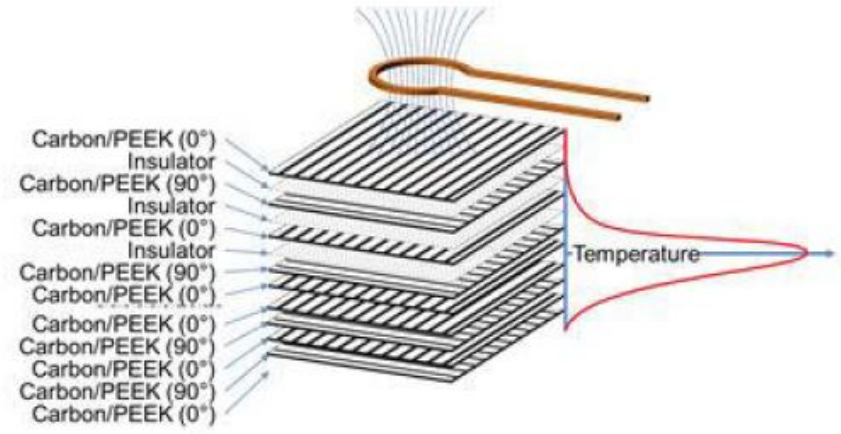

Figure 1.8: Induction heating by integrated susceptor [23]

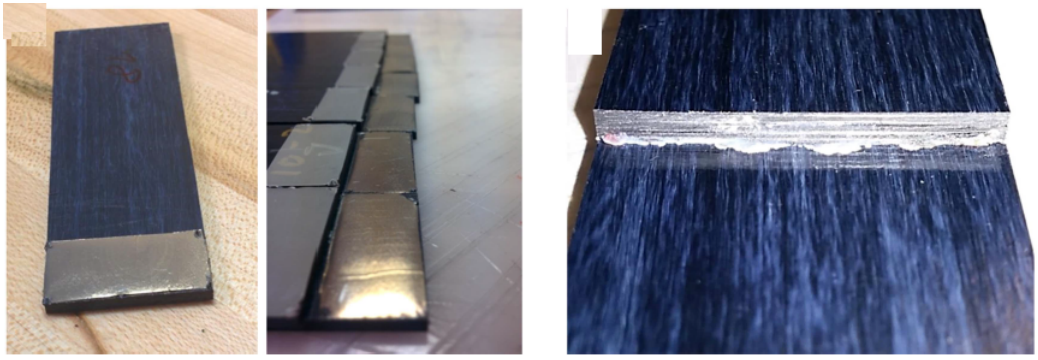

Figure 1.9: Susceptor made of coated nano carbon fiber [24]

In a study done by Danilo et. al [25] copper wires have been integrated in GF-reinforced thermoplastic composites so the need of using susceptor as heating element is eliminated. Figure 1.10 demonstrates this idea [25].

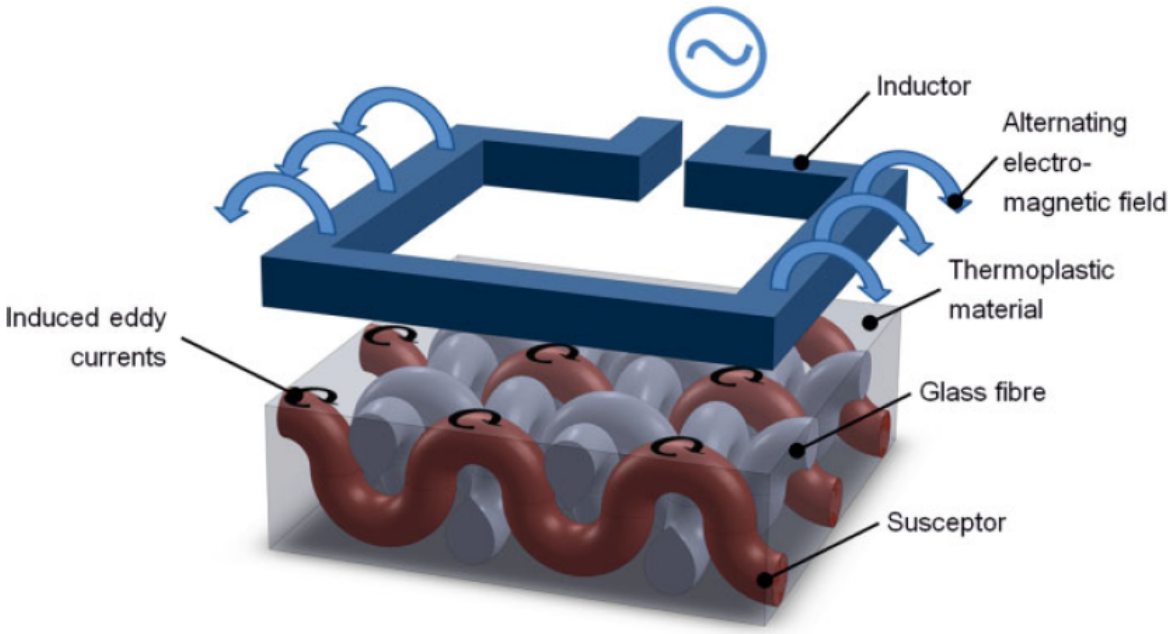

Figure 1.10: Induction heating by integrated susceptor [25]

1.10 Purpose and limitations

Purpose:
Since it was not possible to measure temperature distribution history at the welding interface during experiment using thermal camera. The main purpose of this thesis was to develop a simulation model in order to predict temperature distribution history at the welding interface. One of the goal of this project has been to validate the simulation model. In order to achieve that, an experimental set-up needed to be manufactured, so we can conduct induction welding process and record temperature history using thermocouple at a pinpoint location at welding interface. Another goal was to observe how different GF/PEI composites behaves during welding process compared to carbon fiber thermopolastic composites.

Limitations:
In order to simulate induction welding of thermoplastic composites, it is required to use a multiphysics software where we can couple electromagnetic and heat transfer modules. However, it is not possible to model the complete welding process using current multiphysics software including COMSOL. As mentioned earlier the induction welding process also includes: pressing, intermolecular diffusion and crystallization. As none of the available multiphysics softwares, such as LS-DYNA and COMSOL, have a model for intimate contact to calculate surface contact due to pressing, it is not possible to relate heat transfer and consolidation pressure to intimate contact. Also, these multiphysics software are lacking a model for consolidation & solidification. So considering these limitations, we are only able to model induction heating process for the induction welding. This still allows us to predict temperature distribution history at the welding interface using simulation model built by COMSOL and then validate the model by experiment.

2
Theory

2.1 Eddy current in susceptor

Eddy currents are electrical current loops induced in electrically conductive materials by nearby alternating magnetic field. Electromagnetic phenomena in general are governed by Maxwell's equations [26, 27].

$$\nabla \times \mathbf{B} = \mu_0(\mathbf{J} + \epsilon_0 \frac{\partial \mathbf{E}}{\partial t}) \tag{2.1}$$

$$\nabla \cdot \mathbf{E} = \frac{\rho}{\epsilon} \tag{2.2}$$

$$\nabla \cdot \mathbf{B} = 0 \tag{2.3}$$

$$\nabla \times \mathbf{E} = -\frac{\partial \mathbf{B}}{\partial t} \tag{2.4}$$

where variables and parameters, **B**, **J**, **E**, ρ, ϵ and μ_0 are explained in Table 2.1.

Quantity	Symbol	SI unit	Abbreviation
Magnetic field	**B**	$Tesla$	[T]
Current density (volume)	**J**	$Ampere/meter^2$	$[A/m^2]$
Electric field	**E**	$Volt/meter$	$[V/m]$
Charge density	ρ	$Coulomb/meter^3$	$[C/m^3]$
Permittivity	ϵ_0	$Farad/meter$	$[F/m]$
Permeability	μ_0	$Henry/meter$	$[H/m]$

Table 2.1: Maxwell's equations parameters

Equation 2.1 is Ampere law which describes how a circulating magnetic field is produced by an electric current and by an electric field that changes with time, Equation 2.2 is Gauss's law for electric fields and describes divergence of the electric field and the charge density at the individual points. Equation 2.3 is Gauss's law for magnetic field and explains divergence of magnetic field must be zero. Equation 2.4 is Faraday's law of induction and explains a circulating electric field is produced by a magnetic filed that changes with time [26, 27].

The generation of eddy currents in the susceptor is governed by Amperes and Faraday's laws and respective constitutive relation. The former are usually represented by employing magnetic vector potential **A**.

$$\mathbf{B} = \nabla \times \mathbf{A}. \tag{2.5}$$

Knowing **B** from Equation 2.5, the electric field in the media can be found from Equation 2.4 and the current can be obtained.

Then, from Equation 2.4 and 2.5, it yields

$$\nabla \times \mathbf{E} = -\nabla \times \frac{\partial \mathbf{A}}{\partial t} \tag{2.6}$$

By integrating both sides,it follows

$$\mathbf{E} = -\frac{\partial \mathbf{A}}{\partial t} - \nabla\phi \tag{2.7}$$

where ϕ is the electric scalar potential.

Next step, Equation 2.8 defines Ohm's law as follow

$$\mathbf{J} = \sigma\mathbf{E} \tag{2.8}$$

where σ is electrical conductivity. Accordingly, using Equation 2.7, Equation 2.8 is re-written as

$$\mathbf{J} = -\sigma\frac{\partial \mathbf{A}}{\partial t} - \sigma\nabla\phi \tag{2.9}$$

where $\mathbf{J}_s = -\sigma\nabla\phi$ is the source (excitation) current density [28].

For a frequency domain analysis by assuming sinusoidal wave forms, it is possible to write $\frac{\partial}{\partial t} = i\omega$ and electric field as $\mathbf{E} = i\omega\mathbf{A}$, [29]. Then by placing Equations 2.9 and 2.5 in Equation 2.1 the governing equation in frequency domain becomes

$$(\sigma i\omega + \omega^2\epsilon)\mathbf{A} + \nabla \times [\mu_0^{-1}(\nabla \times \mathbf{A})] = \mathbf{J}_s. \tag{2.10}$$

Equation 2.1 is to be solved for magnetic vector potential **A**. The term $\mathbf{J}_{eddy} = (\sigma i\omega + \omega^2\epsilon)\mathbf{A}$ in Equation 2.10 describes the eddy-current in the susceptor and the right hand side represents the coil current. Accordingly the volumetric heat Q $[W/m^3]$ generated at the susceptor is calculated by

$$\mathbf{Q} = \mathbf{J}_{eddy} \cdot \mathbf{E} \tag{2.11}$$

2.2 Heat transfer model

In order to obtain sufficiently accurate results, a full 3D transient heat transfer analysis is required. According to Lienhard et. al [30], the governing equation for heat conduction is

$$\rho \, C_p \, \frac{\partial T}{\partial t} = Q + \nabla \cdot (k \nabla T) \tag{2.12}$$

where ρ is the material density, C_p is the specific heat capacity, T is the absolute temperature, Q is the rate of heat generation and k is the thermal conductivity. Anistropic heat transfer is assumed for the susceptor and the laminates according to model proposed by Writz et. al [31] and Holms et. al [32]. In addition to conduction, convective and radiation boundary out flux need to be applied. Convective cooling is taken into account on all boundaries in contact with air, and is represented by Equation 2.13.

$$Q_c = h \, (T_b \, - T_\infty) \tag{2.13}$$

where Q_c is the convective out flux, h is the overall heat transfer coefficient. T_b is temperature on the surface and T_∞ is temperature of the surrounding air.

Radiation on the outer boundaries was defined by use of the the Stefan–Boltzmann law for non-black body [30]. Out flux by radiation between body and surrounding air is defined as

$$Q_r = \epsilon \sigma_s \, (T_b^4 \, - \, T_\infty^4) \tag{2.14}$$

where Q_r is the radiation out flux, ϵ is the emissivity, σ_s is the Stefan-Boltzmann constant, T_b is the surface temperature and T_∞ is the temperature of surroundings air.

3

3D Finite Element Induction Heating Model

3.1 Geometry

Geometry presented in the simulation is generated according to the experimental welding setup in Figure 3.1. All domains used in the welding set up are described below.

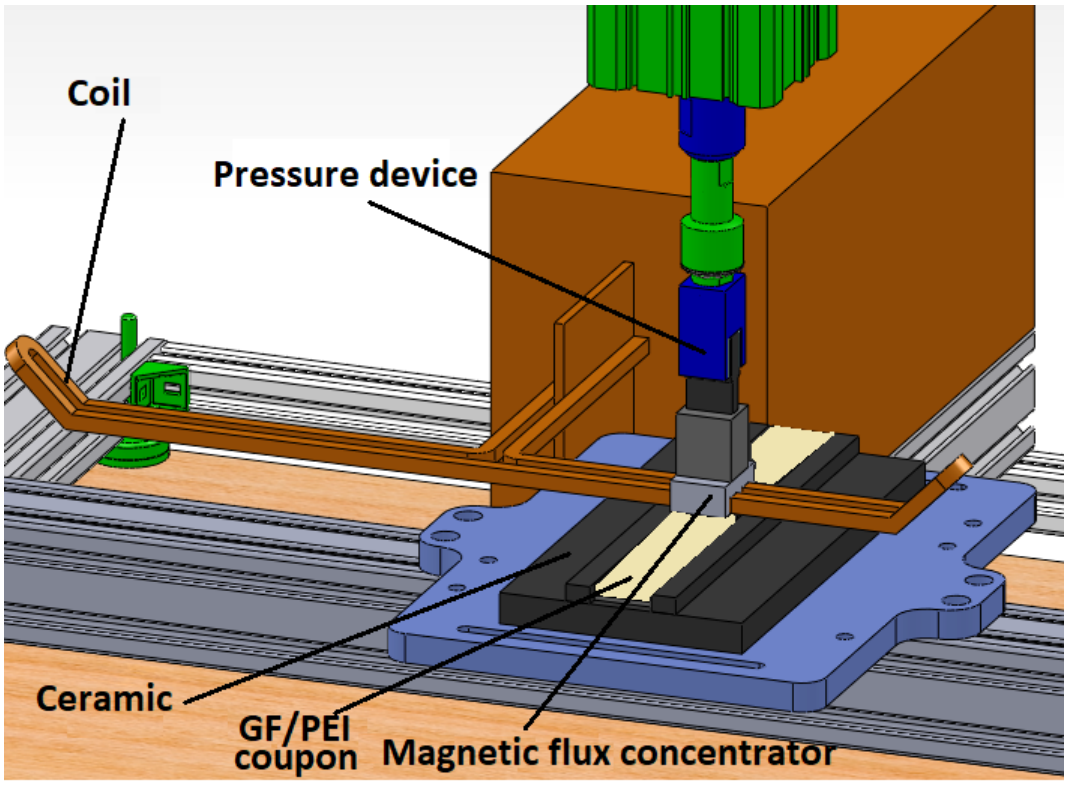

Figure 3.1: Induction welding experimental setup

Domains: Magnetic flux concentrator, ceramic supports, two GF/PEI laminates, two coils, the susceptor and all elements are surrounded by air. Figure 3.2 demonstrates all domains and their arrangements in the welding setup.

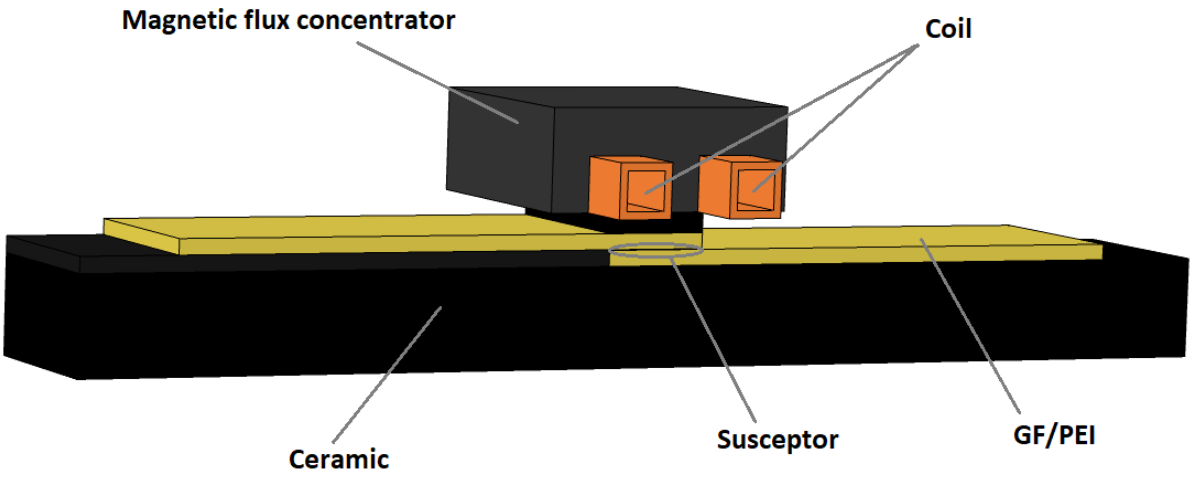

Figure 3.2: Geometry of the welding set up

3.2 Simplifications

Minimizing the complexity of such a complicated multi-physics problem is an important step in modeling induction welding process. Accordingly the following simplifications have been made.

- **Effect of latent heat**: latent heat occurs during crystallisation and crystal melting because of phase change in materials. This heat does not result in raising the temperature in material but just contributes in phase change and breaking bonds between atoms during crystal melting. According to studies by Ageorges et. al [33] it has been observed that the effect of latent heat as result of crystallization has negligible effect on heat transfer at the welding interface. This is due to the fact that only very small portion of material goes through phase change during welding process. Figure 3.3 shows this influence.

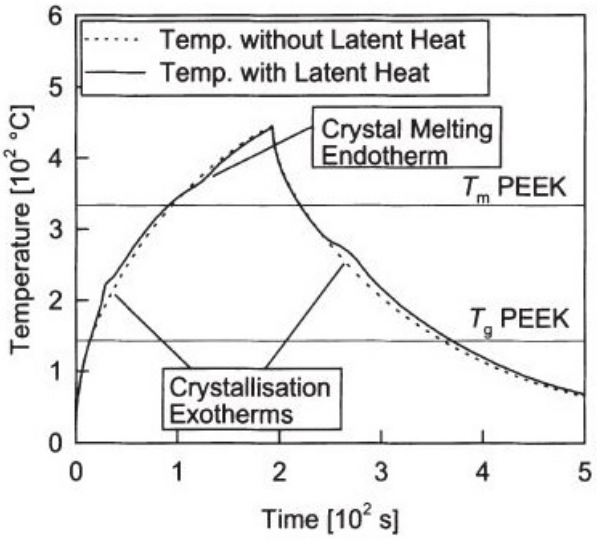

Figure 3.3: Effect of latent heat in fusion bonding 3.3

- **Material model**: in order to provide material properties for COMSOL simulation model, homogenized material properties for the metal mesh susceptor were derived according to Writz et. al [34] were used to calculate effective in-plane thermal and electrical conductivity of susceptor, see section 3.5.3. Also for glass fiber polyetherimide a homogenization heat transfer model according to Holms et. al [32] is used to take into account in plane and out of plane heat conductivity of laminates, see section 3.5.4.
- **Temperature dependent material properties**: Temperature dependent has been implemented for the electrical conductivity.
- **Density**: density of materials used in the process are assumed to be constant.
- **Heating process**: the major heating mechanism in the susceptor is due to resistive heating or joule loss. There is potentially a small contribution of hysteresis loss in the susceptor but this contribution of hysteresis loss is considered negligible.
- **Surface grooves**: surface smoothness has a direct effect on heat conduction between parts. A poor contact due to surface roughness leads to poor heat conduction between parts. This results in heat to be trapped in some parts of the welding set up and lead to sudden raise of temperature.

3.3 Magnetic field

The electrodynamics part of induction welding process is the dominating physics in building simulation model. It is so because of implementation of physics controlled meshing. All domains are considered in magnetic field module (MF) of COMSOL. For the initial values in this module, the magnetic vector potential is set to zero because there is no current in the coil at the time $t = 0$.

3.3.1 Domains

Domains containing magnetic or conductive elements and domains with high permeability play crucial role in the MF module. Important domains to be considered in MF module are therefore: susceptor, magnetic flux concentrator and coil.

Coil: the hollow coil used in the setup has a square cross section.

Magnetic flux concentrator (MFC): the MFC is used in order to curb magnetic fields generated by the coil by keeping the field inside MFC. Concentration of magnetic field also improves proximity effect described previously as it is shown in the Figure 1.7.

Figure 3.4 demonstrates how magnetic field is concentrated due to using magnetic flux concentrator.

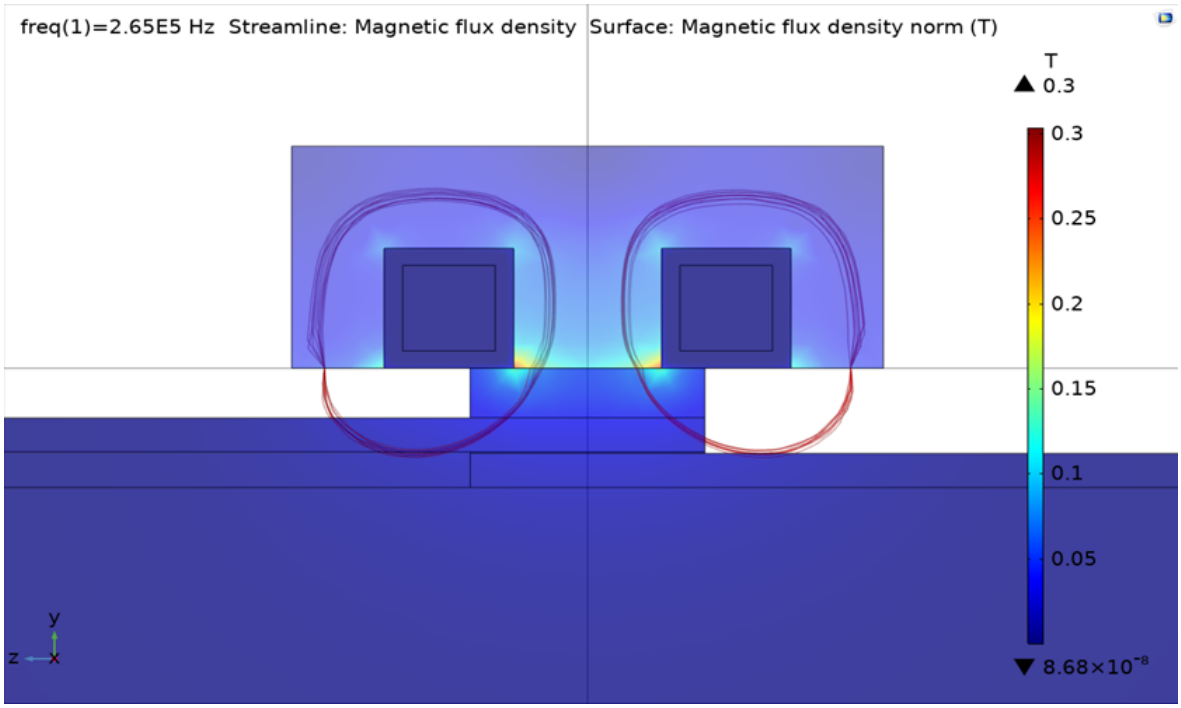

Figure 3.4: Magnetic flux concentrator function

3.4 Boundary conditions

For both MF module and HT module boundary conditions need to be defined according to the experimental set up. In order to do so boundary conditions are divided in two categories and discussed separately for both MF and the HT module.

3.4.1 Electromagnetic boundary conditions

Magnetic insulation:

boundaries of the air domain is considered as magnetic insulation, it means magnetic field can not get through the boundaries of the air domain. In fact COMSOL requires air domain to be defined where ever it needs to calculate the magnetic fields.

Boundaries for coil current:

Both ends of each coil are assigned to a current of 471 Ampere. Directions of the current in the coils are opposite. Figure 3.5 demonstrates how currents are introduced for coils.

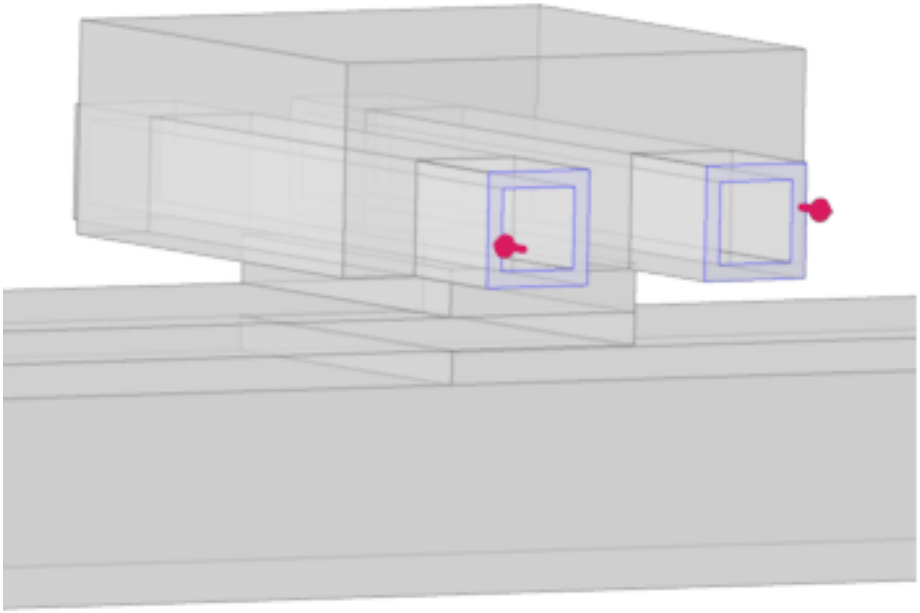

Figure 3.5: Current introduced in the boundaries of coils

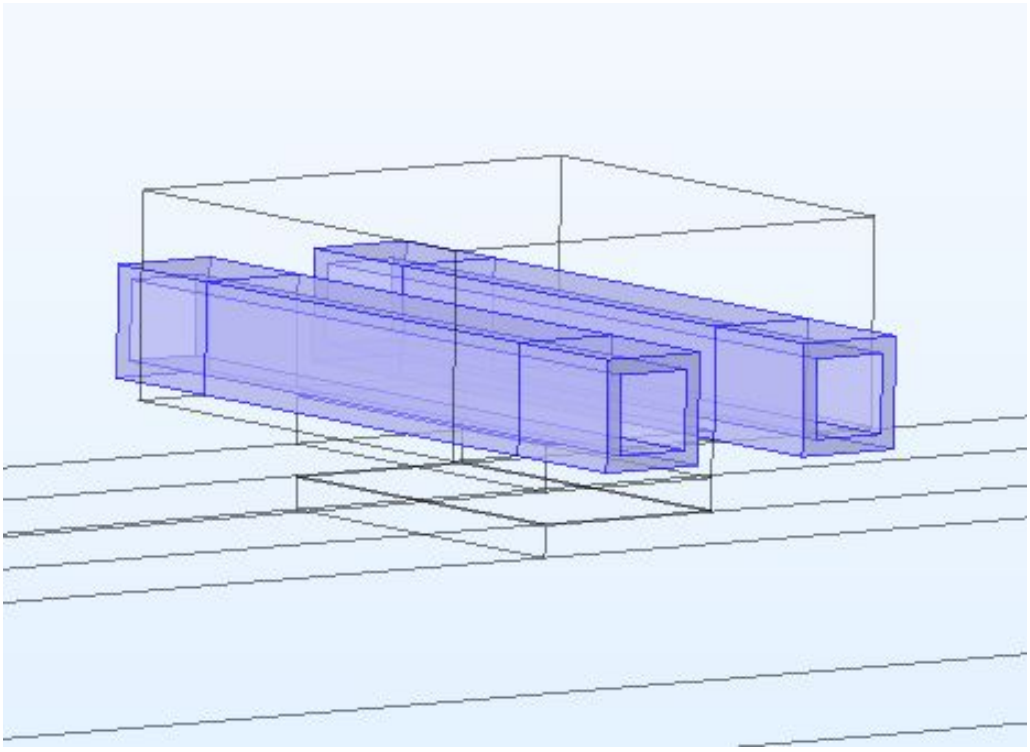

Figure 3.6: Temperature introduced to the boundaries of coil

3.4.2 Heat transfer boundary conditions

Conduction:

- For all solid surfaces in contact with each other such as; ceramics, coil, flux concentrators, laminates and susceptor thermal flux continuity is assigned.
- Since temperature of coil increases to 370 Kelvin, all boundaries of the coil is set to this temperature. Figure 3.6 shows how boundaries are chosen. The coil is water cooled so the temperature of the coil does not exceed 370 Kelvin.
- Initial temperature for all surfaces in other domains including: magnetic flux concentrator, ceramics, GF/PEI samples and Susceptor are set to room temperature, 293 Kelvin.

Radiation: radiation cooling is assigned to all surfaces in contact with air. The constant of surface emissivity is chosen as $\epsilon = 0.9$ according to Tolbot et. al [35].
Convection:
Heat flux for convection cooling is also assigned to all surfaces in contact with the air, the constant for the heat transfer coefficient is set to $h = 5\frac{W}{(m^2.K)}$ according to Talbot et. al [35].

3.5 Material properties

In order to predict the behavior of the materials in an electromagnetic environment, which results in heat generation, both electromagnetic and thermal material properties need to be defined. Values for material properties were taken from literature and material suppliers.

3.5.1 Coil

Electromagnetic and thermal material properties for both coil domains are provided as input for simulation model as in Figure 3.7. Physically there is one coil, but in order to reduce the size of model two coil domains are used in the model. The coil is made of 99% pure copper and the material properties are taken from COMSOL library.

Property	Value	Unit
Relative permeability	1	1
Electrical conductivity	5.998e7[S/m]	S/m
Coefficient of thermal expansion	17e-6[1/K]	1/K
Heat capacity at constant pressure	385[J/(kg*K)]	J/(kg·K)
Relative permittivity	1	1
Density	8960[kg/m^3]	kg/m^3
Thermal conductivity	400[W/(m*K)]	W/(m·K)

Figure 3.7: Coil material properties

3.5.2 Magnetic flux concentrator

Electromagnetic and thermal material properties for MFC are provided as input for simulation model according to Table 3.1. The Magnetic flux concentrator is called Ferrotron 559H and is manufactured by Fluxtrol. Material properties are provided by manufacturer.

Symbol	**Property**	**Unit**	**Value**
μ_r	Relative permeability	1	18
σ	Electrical conductivity	S/m	10
ϵ_r	Relative permittivity	1	1
k_T	Thermal conductivity	$W/(m.K)$	4
σ	Density	kg/m^3	1000
C_p	Heat capacity at constant pressure	$J/(kg.K)$	1000

Table 3.1: Magnetic flux concentrator material properties

3.5.3 Susceptor

The susceptor used is a plain weave mesh with wire diameter of $40\mu m$ and open gap width of $90\mu m$. This square woven metal mesh susceptor is made of stainless steel 304. Figure 3.8 demonstrates the susceptor used for this set up [35]. Table 3.2 shows dimensions of susceptor, such as diameter of filament etc.

Variable	**Dimention**	**Value**
dx	wire diameter (x-direction) (mm)	0.040
dy	wire diameter (y-direction) (mm)	0.040
Mx	number of wires in x-direction	200
My	number of wires in y-direction	200
C_f	compression factor	1
n	number of screen	1
$Length$	(mm)	25.4
$width$	(mm)	12.7

Table 3.2: Susceptor dimensions

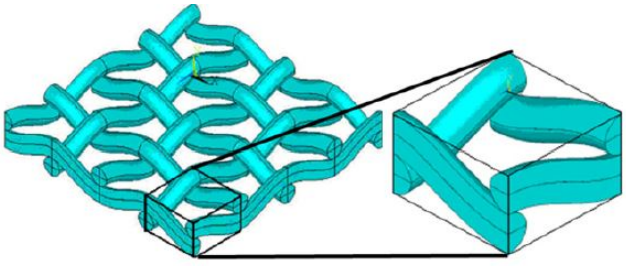

Figure 3.8: Susceptor cell unit [35]

Material properties of 304 stainless steel are available [35], however the equivalent or homogenized material properties of metal mesh net stainless steel with PEI polymer in the gaps needs to be calculated as this is not predefined in COMSOL.

Symbol	**Property**	**Unit**	**Value**
ρ	Density	(kg/m3)	8000
C_p	Specific heat	(J/kg.K)	500
k_T	Thermal conductivity	(W/m.K)	16.2
σ	Electrical conductivity	$1/\Omega.m$	714285

Table 3.3: Stainless steel 304 material properties

Material properties provided in Table 3.3 can not be used directly in the simulation model for the susceptor, because we have gaps in the susceptor which are filled with PEI polymer, so here in fact we have a mixture of stainless steel and polymer and we need to address material properties according to this mixture. Homogenized or effective material properties must be derived according to the dimensions provided in Table 3.2. In order to calculate effective material properties, in-plane effective thermal and electrical conductivity of plain-weave metal mesh is calculated according to Writz et. al [31]. Thermal conductivity by Equation 3.1 and electrical conductivity is calculated by Equation 3.2.

$$k = \frac{L}{R_H \cdot A} \tag{3.1}$$

$$\sigma = \frac{A \cdot R_E}{L} \tag{3.2}$$

where L is the length of element, A is cross section area and R_H is thermal resistance and R_E is electrical resistivity.

Compression factor is defined by $C_f = t/(n_{layer} \cdot 2d)$, where t is the thickness of the metal mesh susceptor, n_{layer} number of layers and d diameter of wires. For the susceptor used it is assumed that compression factor is $C_f = 1$ and diameter of wires in both x-direction and y-direction are equal, $d_x = d_y$. Figure 3.9 demonstrates schematic of unit cell as well as wire diameters.

Since wire diameters are the same, in order to calculate in plane heat and electrical conductivity there is no need to split in plane conductivity in two parts for x and y directions. Here we assume that PEI polymer and susceptor are embedded in each other.

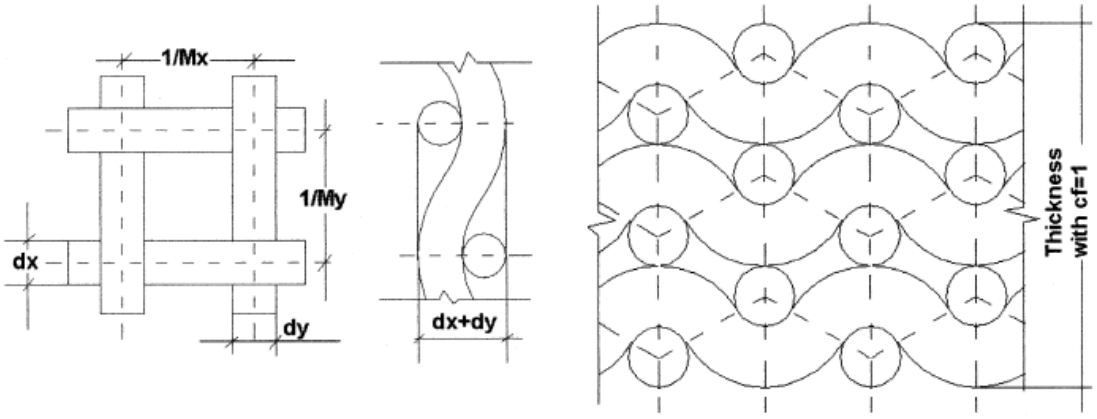

Figure 3.9: one unit cell of the metal mesh susceptor [31]

In order to simplify the calculations, the true unit cell is approximated by a simple geometry according to Figure 3.10. This helps to derive the related thermal circuits associated to one cell unit for both in plane and out of plane thermal conductivities. The wire filament lengths in unit cell needs to be calculated by Equation 3.3 according to Writz et. al [31].

$$S_{x,y} = \frac{1}{M_x}[1 + 9.6(\frac{d_y.M_x}{4})^2 - 49.2(\frac{d_y.M_x}{4})^2] \tag{3.3}$$

Thermal circuit associated to in plane heat conductivity for one unit cell shown in Figure 3.11 is demonstrated in Figure 3.12.

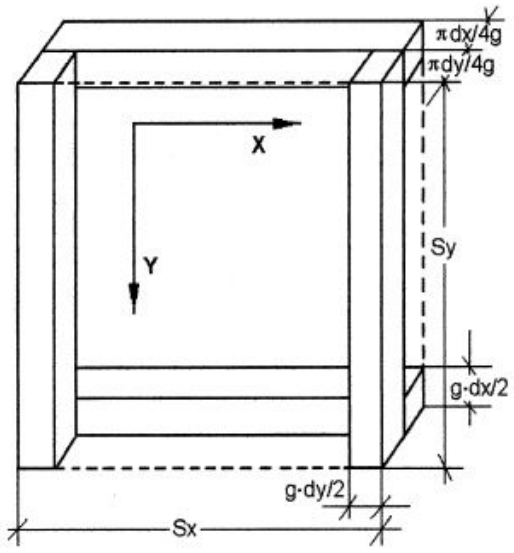

Figure 3.10: Transformed unit cell [31]

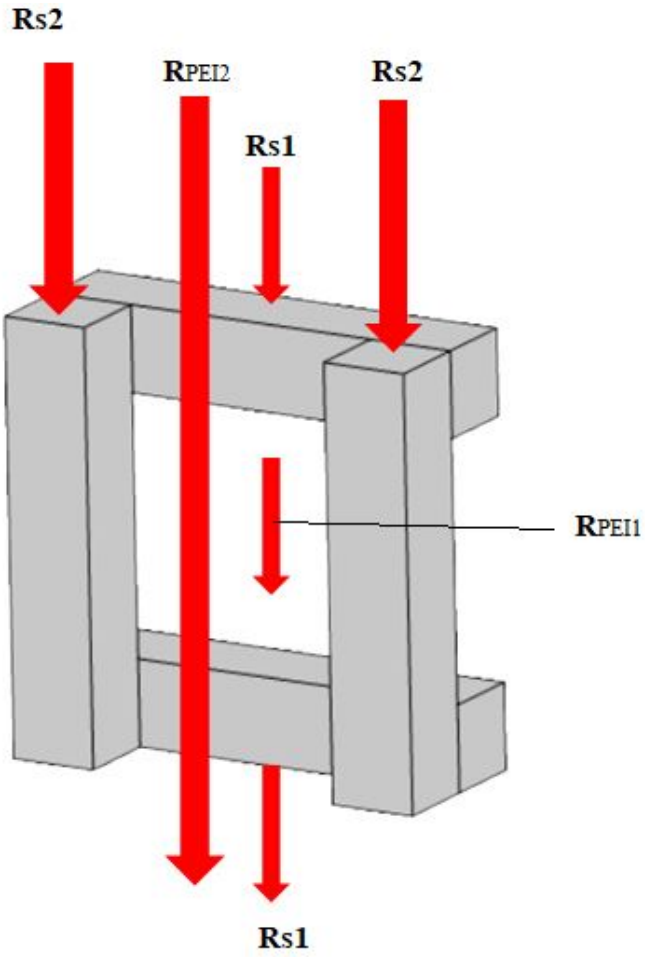

Figure 3.11: In plane thermal configuration for one cell

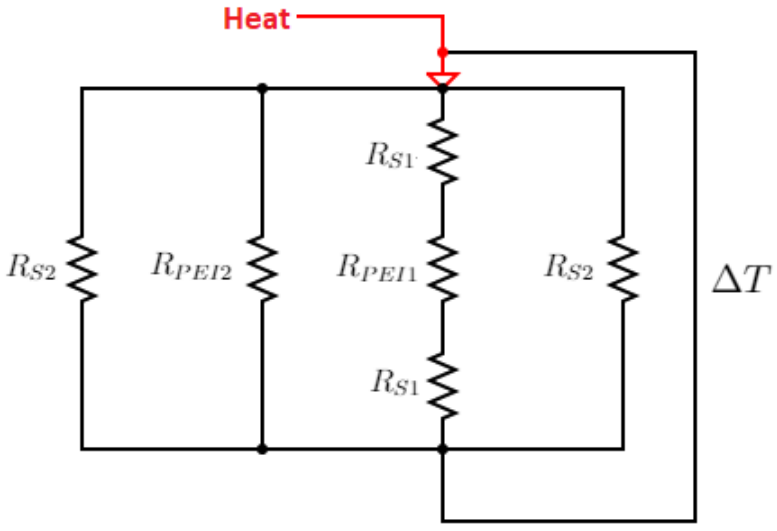

Figure 3.12: In plane thermal circuit of one unit cell of the metal mesh susceptor

To calculate thermal resistance for each pathway Equation 3.4 is used.

$$R_H = \frac{L}{k \cdot A} \tag{3.4}$$

where L is the length of the element and k is thermal conductivity. According to Equation 3.1, R_{PEI} is thermal resistance for PEI polymer and R_S thermal resistance for stainless steel wire presented by equations below

$$R_{PEI} = \frac{L}{k_{PEI} \cdot A} \tag{3.5}$$

$$R_S = \frac{L}{k_S \cdot A} \tag{3.6}$$

According to Figure 3.12, total thermal resistance for x or y directions (in-plane heat conductivity) is

$$\frac{1}{R_{x,y}} = \Big(\frac{2}{R_{S2}} + \frac{1}{R_{PEI2}} + \frac{1}{2R_{S2} + R_{PEI1}}\Big) \tag{3.7}$$

where R_{S2} , R_{S1} , R_{PEI1} and R_{PEI2} are defined by equations below, where $g = \frac{\pi}{4-C_f}$, according to Writz at. al [31].

$$R_{S2} = \frac{2g^2}{k_s \ \pi \ S_x} \tag{3.8}$$

$$R_{S1} = \frac{8S_x}{k_s \ \pi \ dy^2} \tag{3.9}$$

$$R_{PEI1} = \frac{4g \ (S_x - g.dx)}{k_{PEI} \ \pi \ dy^2} \tag{3.10}$$

$$R_{PEI2} = \frac{4g \ S_x}{(k_{PEI} \ \pi \ dy) \times (S_x - g \ dy)} \tag{3.11}$$

In the next step, it is required to calculate out-of-plane heat and electrical conductivity. Thermal circuit associated to out-of-plane heat conductivity for one unit cell shown in Figure 3.13 is demonstrated in Figure 3.14.

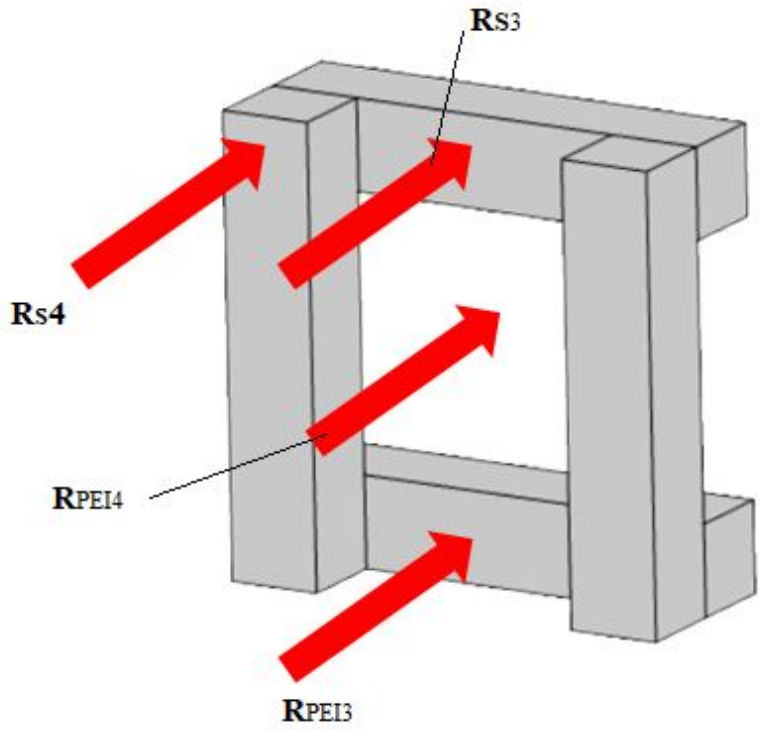

Figure 3.13: out-of-plane thermal thermal configuration for one cell

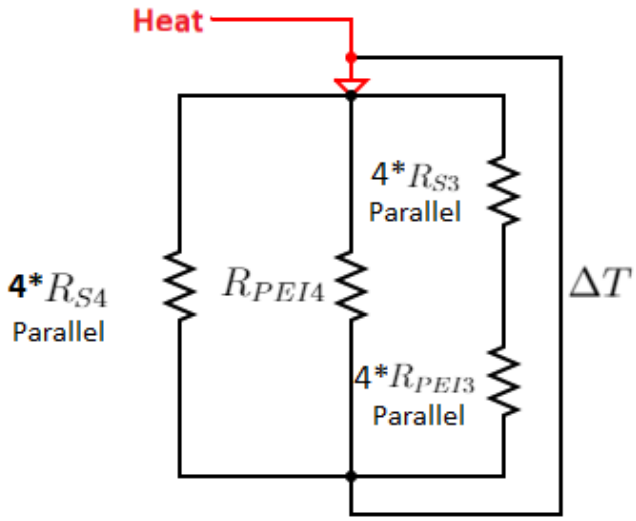

Figure 3.14: out-of-plane thermal circuit for one unit cell of the metal mesh susceptor

Accordingly effective thermal resistance for out-of-plane cell is calculated by the following equation

$$\frac{1}{R_Z} = \left(\frac{4}{R_{S4}} + \frac{1}{R_{PEI4}} + \frac{4}{R_{S3} + R_{PEI3}}\right) \tag{3.12}$$

where R_{S3}, R_{PEI3}, R_{PEI4} and R_{S4} are defined as follow

$$R_{S3} = \frac{\pi}{k_S(S_x - g\ dx) \cdot g\ 2g^2} \tag{3.13}$$

$$R_{PEI3} = \frac{\pi}{k_{PEI}(S_x - g\ dx) \cdot g\ 2g^2} \tag{3.14}$$

$$R_{PEI4} = \frac{\pi.dx}{k_{PEI}(S_x - g\ dx)(S_x - g\ dx)2g} \tag{3.15}$$

$$R_{S4} = \frac{2\pi}{k_S\ g^3\ dx}. \tag{3.16}$$

In order to calculate equivalent density and equivalent specific heat rule of mixture is incorporated. Equation 3.17 calculates equivalent density for susceptor and PEI. Equation 3.18 is used to calculate the equivalent specific heat for the susceptor.

$$\rho_{susceptor} = \rho_{steel} \cdot V_{steel} + \rho_{PEI} \cdot V_{PEI} \tag{3.17}$$

$$c_{P,susceptor} = \frac{\rho_{steel}\ \cdot\ V_{steel}\ \cdot\ c_{P,steel}\ + \rho_{PEI}\ \cdot\ V_{PEI}\ \cdot\ c_{P,PEI}}{\rho_{susceptor}} \tag{3.18}$$

where ρ_{steel} and ρ_{PEI} are respectively the density of stainless steel 304 and polyetherimide matrix. V_{steel} and V_{PEI} are respectively the volume fraction for stainless steel and polyetherimide matrix.

In order to calculate the thickness of the susceptor according to Xu et. al [31], Equation 3.19 is used.

$$t_n = n\ C_f \cdot (dx + dy) \tag{3.19}$$

where n=1 is number of screens.

Effective material properties for the susceptor embedded in PEI polymer are provided in Table 3.4.

Symbol	Property	Unit	Value
ρ	Density	(kg/m3)	2955
$k_{x,y}$	Thermal conductivity (in plane)	(W/m.K)	2.1
k_z	Thermal conductivity (out of plane)	(W/m.K)	1.1
σ	Electrical conductivity	$1/\Omega.m$	84465
V_{steel}	Volume fraction V_{steel}	-	25/100
C_p	Specific heat	$J/(kg \cdot K)$	1000

Table 3.4: Effective material properties for susceptor

Temperature dependent electrical resistivity:

In order to take into account temperature dependent material properties, conductivity of the susceptor is defined as a function of temperature according to Figure 3.15, based on information provided by manufacturer.

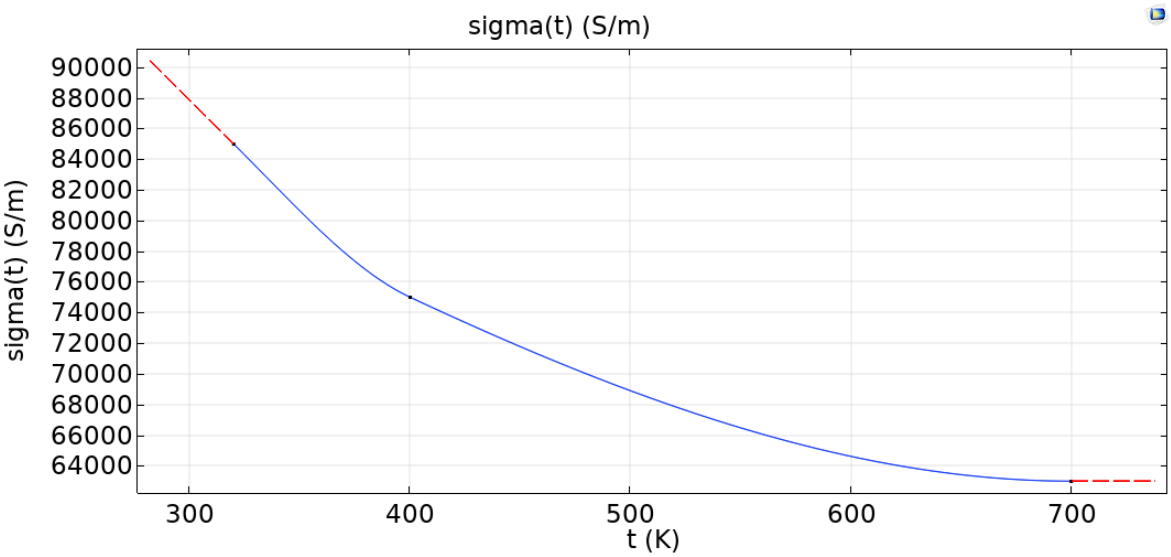

Figure 3.15: Temperature dependent conductivity of the susceptor

3.5.4 Glass fiber polyetherimide laminates

Samples used in the experiment are cut from laminates made of 8 plies. Each ply is made of 8 harness satin weave glass fiber. Figure 3.16 demonstrates the glass fiber arrangements in one ply.

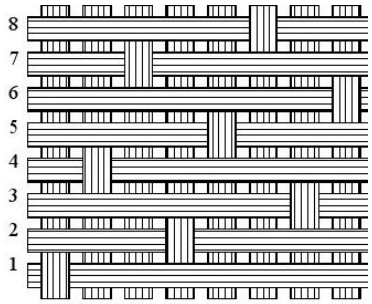

Figure 3.16: 8 harness satin weave glass fiber [36]

In order to find material properties for the laminate, PEI polymer as well as glass fibers needs to be homogenized as one solid element. To do so, a heat transfer material model according to Holms et. al [32] is used. Using rule of mixture longitudinal thermal conductivity of the laminate is calculates by Equation 3.20.

$$k_L = k_{Lf} V_{Gf} \; + \; k_{PEI} V_{PEI} \tag{3.20}$$

where V_{Gf} is volume fraction for glass fiber, V_{PEI} is the volume fraction for PEI polymer, k_{PEI} is the thermal conductivity of PEI polymer, k_{Lf} is longitudinal heat conductivity of glass fiber. Here longitudinal and transverse heat conductivity of glass fiber, k_{Tf} are assumed equal, $k_{Lf} = k_{Tf}$.

For transverse heat conductivity of the laminate, inverse rule of mixture is used according to equation 3.21.

$$\frac{1}{k_T} = \frac{V_{Gf}}{k_{Lf}} \; + \; \frac{V_{PEI}}{k_{PEI}}. \tag{3.21}$$

Since there are 8 satin weave plies (equivalent to 16 unidirectional plies) as the quasi-isotropic stacking sequence and plies are arranged is $[90, 0]_{4s}$ configuration, it is important to calculate each layer's conductivity through a standard coordinate transformation.

$$\begin{bmatrix} k_{11} \\ k_{22} \end{bmatrix} = \begin{bmatrix} m^2 & n^2 \\ n^2 & m^2 \end{bmatrix} \begin{bmatrix} k_L \\ k_T \end{bmatrix} \tag{3.22}$$

where k_{11} and k_{22} are transformed thermal conductivities in the standard coordinate system. $m = \cos\theta$ and $n = \sin\theta$. In order to calculate effective thermal conductivity of the laminate for all the plies Equation 3.23 is used.

$$k_x = k_y = \sum_{n=1}^{N} \frac{h_n}{h} [k_{11}]_n \tag{3.23}$$

The obtained effective heat conductivity and homogenized material properties of GF/PEI laminate are provided in Table 3.5.

Symbol	Property	Unit	Value
ρ	Density	(kg/m3)	1910
$k_{x,y}$	Thermal conductivity (in plane)	(W/m.K)	0.540
k_T	Thermal conductivity (out of plane)	(W/m.K)	0.371
v	Volume fraction	1	0.5
C_p	Specific heat	J/(kg · K)	1263

Table 3.5: Effective material properties for GF/PEI laminate

3.6 Mesh

Due to having multi physics problem, different mesh densities for different domains are required to solve the problem. The mesh sequence is prioritized according to domains requiring highest density mesh. Figure 3.17 demonstrates how different domains are prioritized.

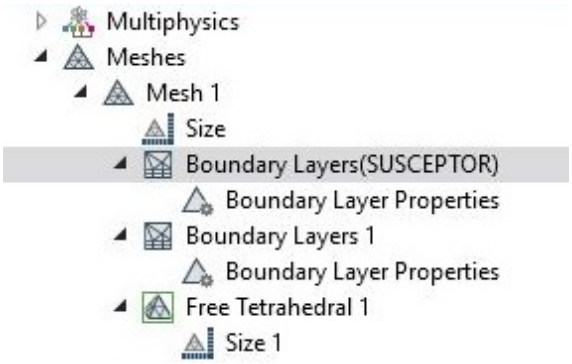

Figure 3.17: Meshing sequence

Here, the susceptor acts as a heat source. Due to high frequency of the alternating magnetic field generated by the coil, this results in micro level skin-depth in the susceptor, where eddy-currents are formed. In order to have sufficient accuracy in calculating eddy currents, at least two element should be fit within the skin-depth in the susceptor. The estimated skin-depth is:

$$\delta = \sqrt{\frac{2\rho}{\mu\omega}} = 3.77 \times 10^{-5} m \tag{3.24}$$

Accordingly, boundary layer with the thickness of $1.5 \times 10^{-5} m$ for all sides of susceptor is used.

The second priority in mesh tree sequence is the coil, where boundary element is used. Figure 3.18 demonstrates coil mesh and boundary layers in its cross section.

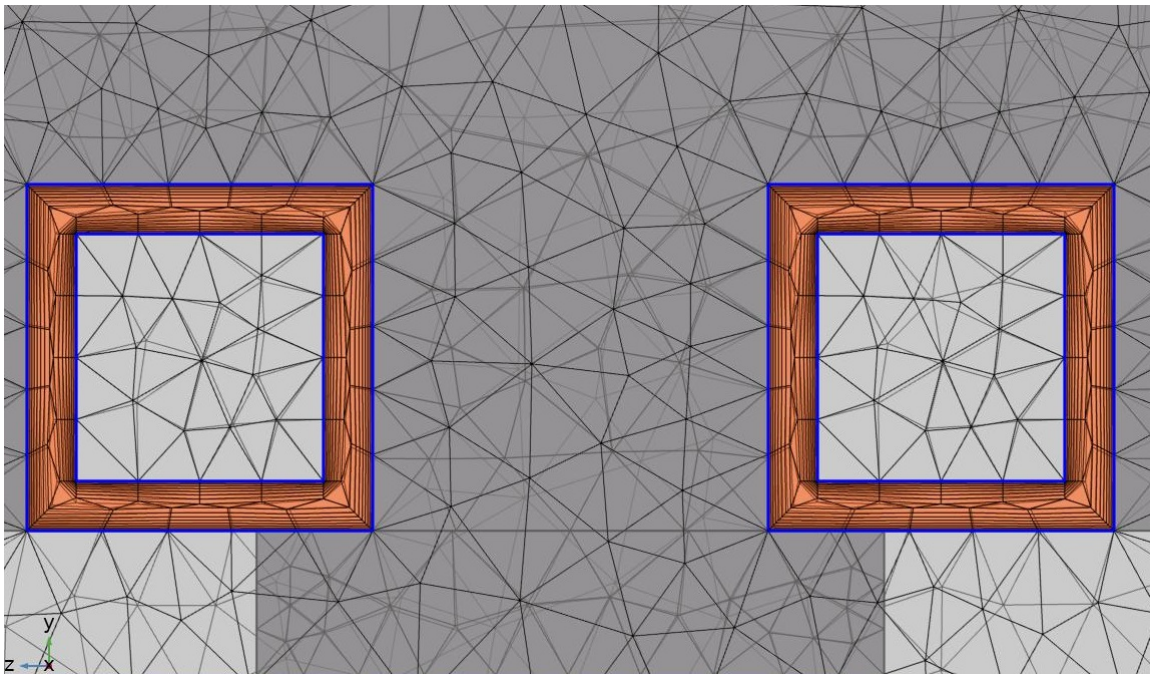

Figure 3.18: Coil boundary mesh

For other domains including; laminates, ceramics, magnetic flux concentrator and air, free tetrahedral elements is used. Figure 3.19 demonstrates the final mesh of all domains. Total number of elements are 153668 and the number of degrees of freedom is 1705413.

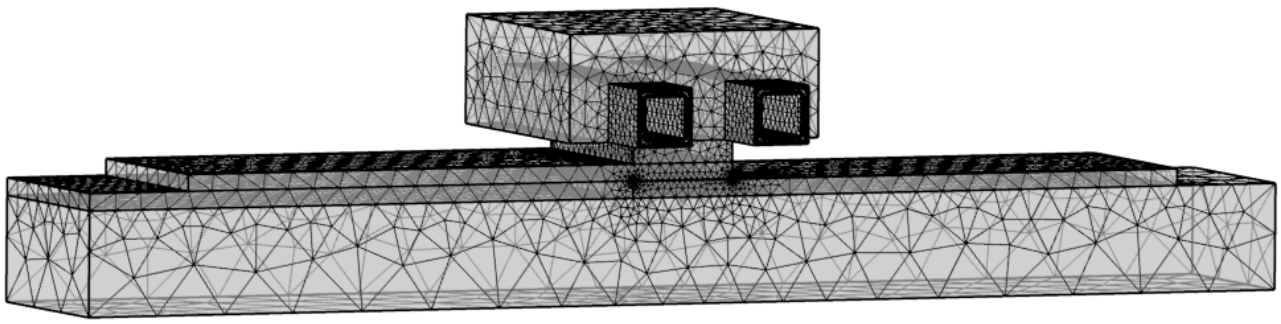

Figure 3.19: Final mesh

Simulation model flowchart

Figure 3.20 demonstrates a flowchart of both way coupling heat transfer and electromagnetic module in COMSOL multiphysics used to build simulation model.

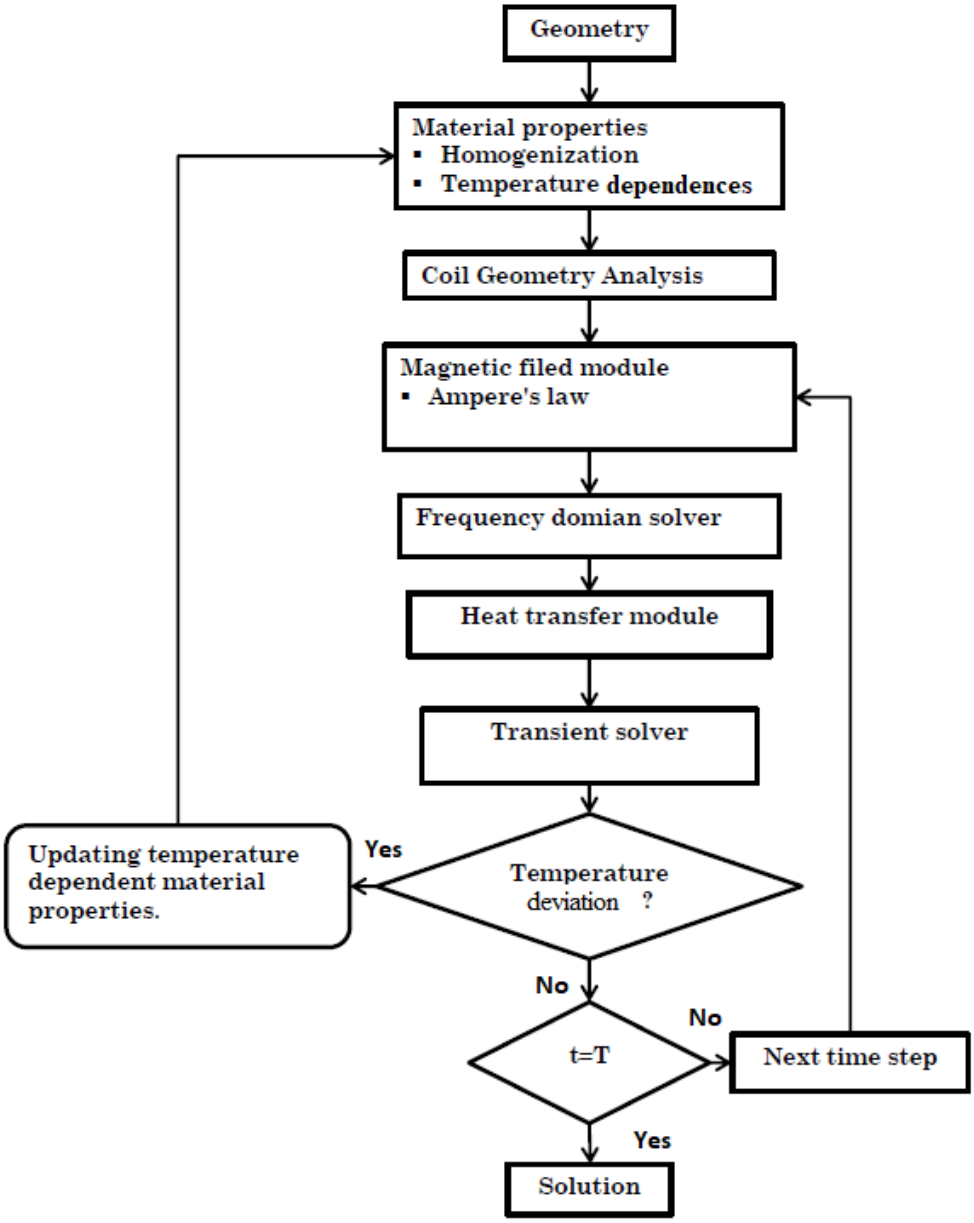

Figure 3.20: Simulation algorithm in COMSOL multiphysics

- First geometry is defined
- Temperature dependent material properties are called.
- Coil geometry analysis calculates the current density in the coil.
- Magnetic field module calculates the magnetic field and eddy currents.
- Heat transfer module calculates the temperature at all domains by considering conduction, radiation and convection.
- The first condition in the flowchart checks if there is any increase in the temperature compared to previous time step. If "Yes" it requests for updated material properties according to the new temperature, if "No" it goes for the next time step. Then the second condition checks if the duration of simulation is finished.

3.7 Numerical results

In order to have a clear image of induction heating and heat distribution process in different component of welding jig, it is important to follow up steps which dominate heat generation process.

3.7.1 Eddy-current

According to Faraday's law alternating magnetic field produces electric field within the susceptor, this electric field induces electric current in the susceptor which according to Ohm's law results in heat generation by joule losses. Figure 3.21 demonstrates eddy current distribution in the susceptor. The pattern of eddy current density is affected by the geometry of the coil as well as the proximity between the coil and the susceptor.

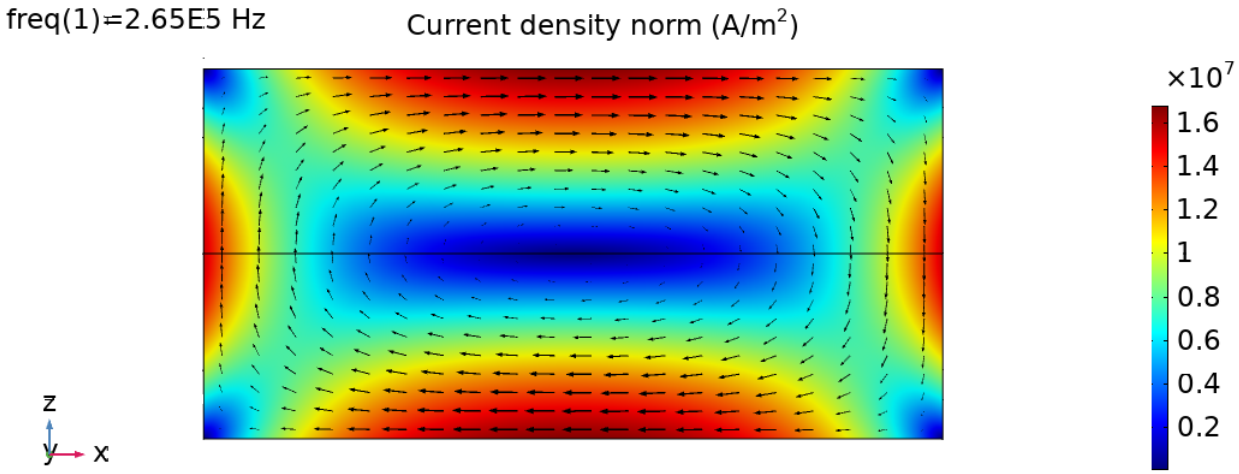

Figure 3.21: Eddy-current distribution on susceptor

Figure 3.21 shows four spots on the susceptor with high concentration of eddy currents. These areas might be locations with high temperature gradients.

3.7.2 Volumetric heat generation and temperature

It is important to identify volumetric heat generation pattern on the susceptor. This can help to predict spots with high temperature gradient. Figure 3.22 demonstrates volumetric heat generation of the susceptor. As expected this pattern correlates well with the eddy current distribution.

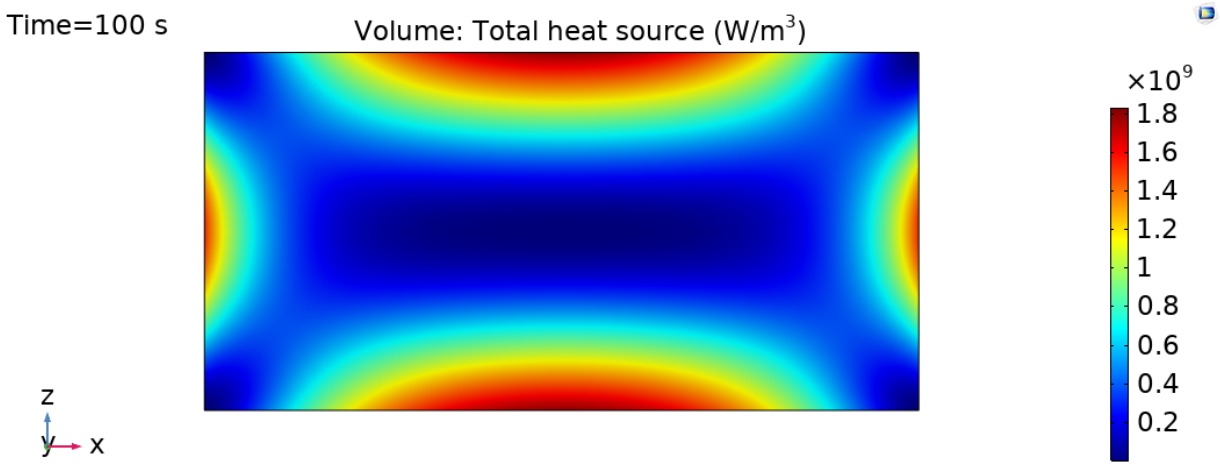

Figure 3.22: Volumetric heat source in susceptor

Figure 3.23 demonstrates the temperature distribution on the susceptor. As it can be observed temperature pattern is different from eddy current distribution and volumetric heat generation. The reason for lower temperature gradient on the upper side of the susceptor is because of the welding jig configuration. In fact, for the upper side of susceptor there is a ceramic support for the sample which also acts as a heat sink therefore reducing the temperature gradient.

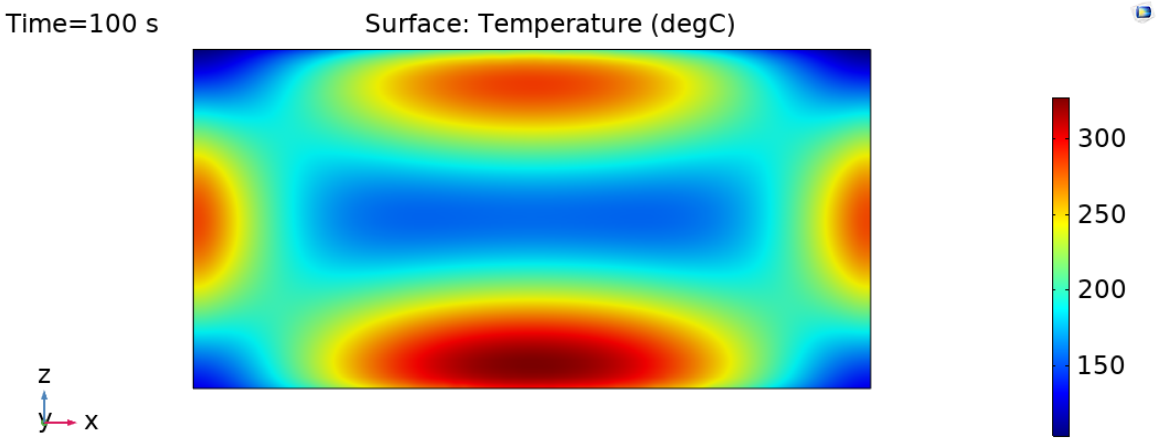

Figure 3.23: Temperature distribution in susceptor

Figure 3.24 provides a side view of the heat distribution in the GF/PEI samples and Figure 3.25 demonstrates in plane heat distribution on the top surface of the GF/PEI sample. As it can be observed areas with high temperature gradient in the susceptor are directly affecting samples. These areas are prone to thermal degradation as it is later shown in experimental part.

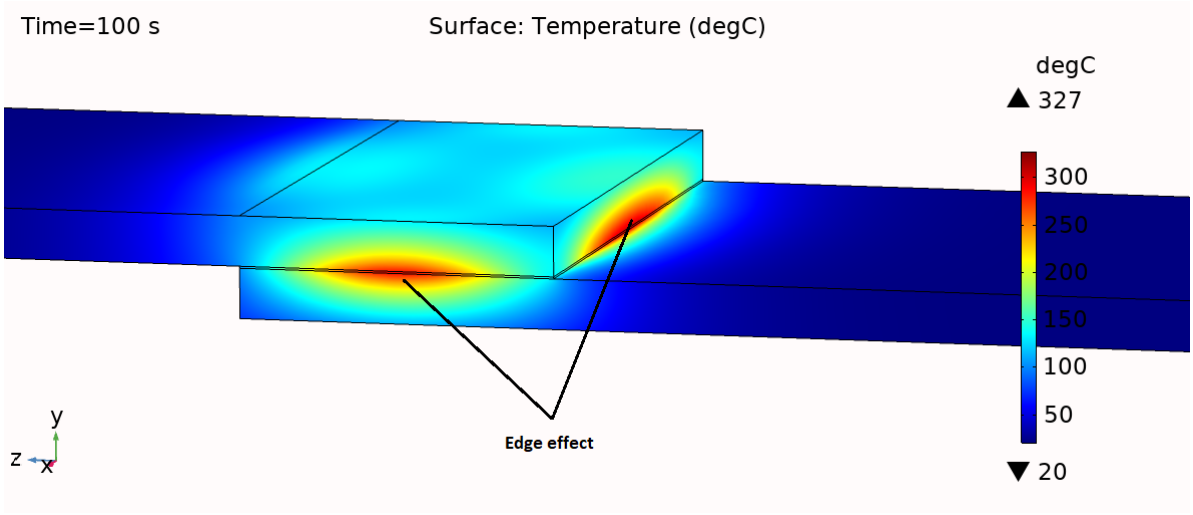

Figure 3.24: Temperature distribution in samples from susceptor

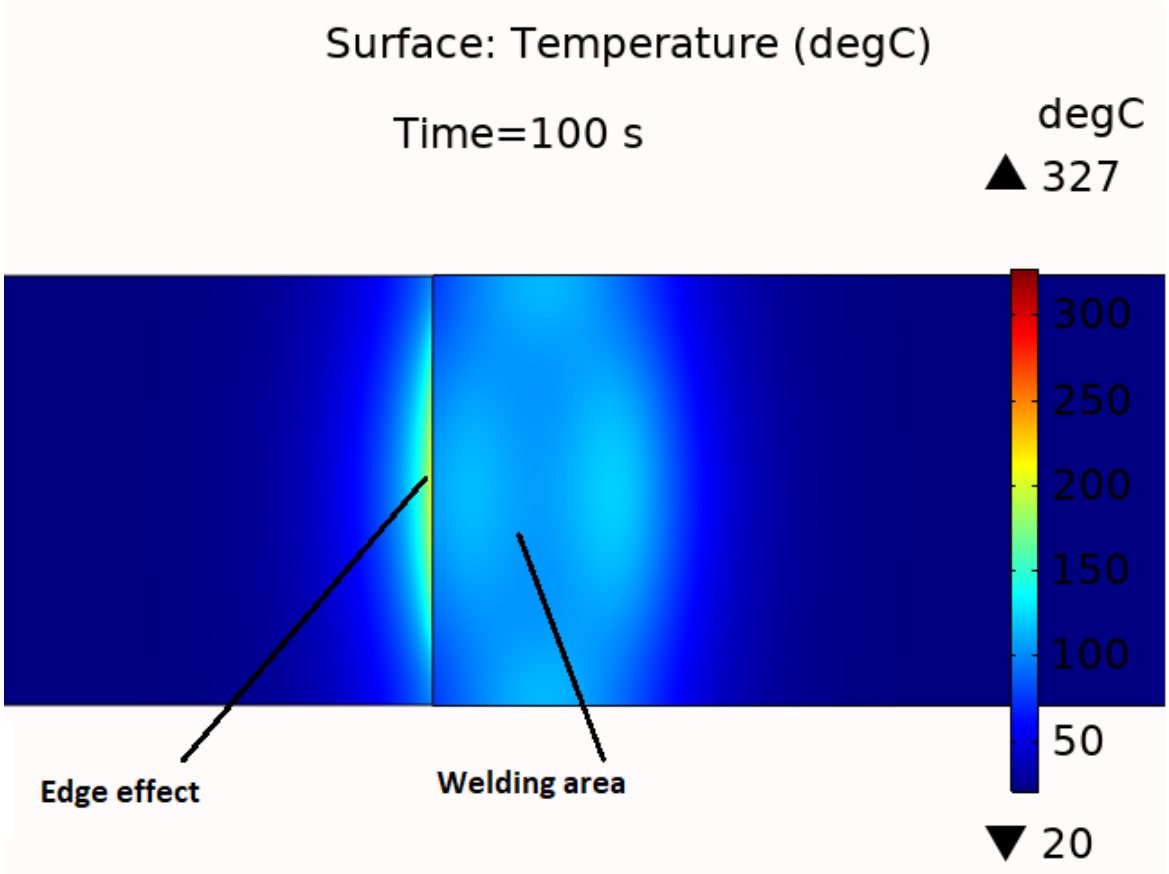

Figure 3.25: View of temperature distribution in the top surface of the GF/PEI sample

3.7.3 Sensitivity analysis

The goal of the sensitivity analysis is to understand which parameters have most influence in the heat generation process. According to a study done by Moser et. al [21], among machine parameters, frequency, coil current and coupling distance have significant effect on temperature deviation. The electrical conductivity, relative permeability, thermal conductivity and heat capacity have by far less influence. Results for sensitivity studies for parameters such as, frequency, coupling distance, coil current, electrical conductivity, heat conductivity and heat capacity, C_p are therefore presented below. For this sensitivity study each parameter is varied by -20%, -10%, 10% and 20% around the reference value.

The reference for the evaluation of parameters variation on induction heating of the susceptor is the average temperature of the susceptor after 60 seconds of heating. The reference machine parameters for this sensitivity study are according to Table 3.6 and 3.7.

For this sensitivity analysis only one parameter at the time is varied and other parameters were kept fixed.

Variation %	**Coil curent [A]**	**Coupling distance [mm]**	**Frequency [khz]**
+20	565	6	3.17
+10	518	5.5	2.91
0	471	5	2.65
-10	424	4.5	2.39
-20	377	4	2.13

Table 3.6: Machine parameter variation for sensitivity analysis

Variation %	**Cp [J/(kg · K)]**	**Heat cond [W/(m · K)]**	**Electric cond [S/m]**
+20	1217	$k_{x,y}$=2.59 , k_z=1.31	92400
+10	1116	$k_{x,y}$=2.37 , k_z=1.21	84700
0	1015	$k_{x,y}$=2.16 , k_z=1.1	77000
-10	914	$k_{x,y}$= 1.94 , k_z= 0.99	69300
-20	813	$k_{x,y}$=2.59 , k_z= 0.88	61600

Table 3.7: Material properties variation for sensitivity analysis

3.7.3.1 Sensitivity analysis result

Frequency: Figures 3.26 and 3.27 demonstrate the influence of frequency on average temperature of the susceptor. The deviation of 10.5% for 10% increase in frequency is observed. Accordingly, we can categorize coil frequency as a parameter with high importance.

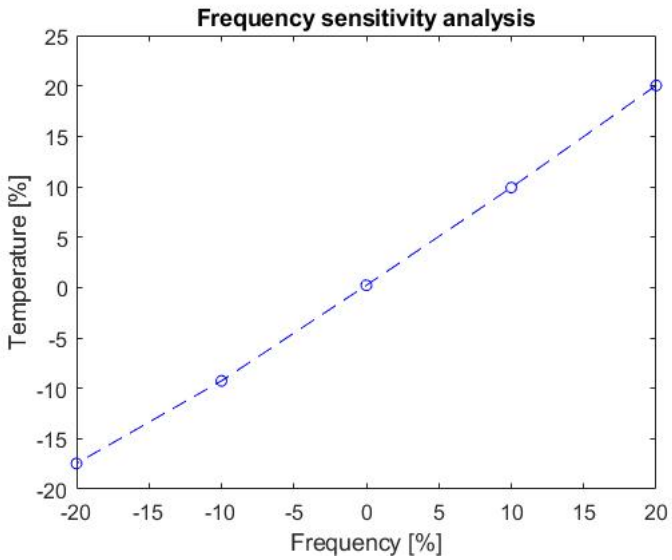

Figure 3.26: Sensitivity analysis for frequency

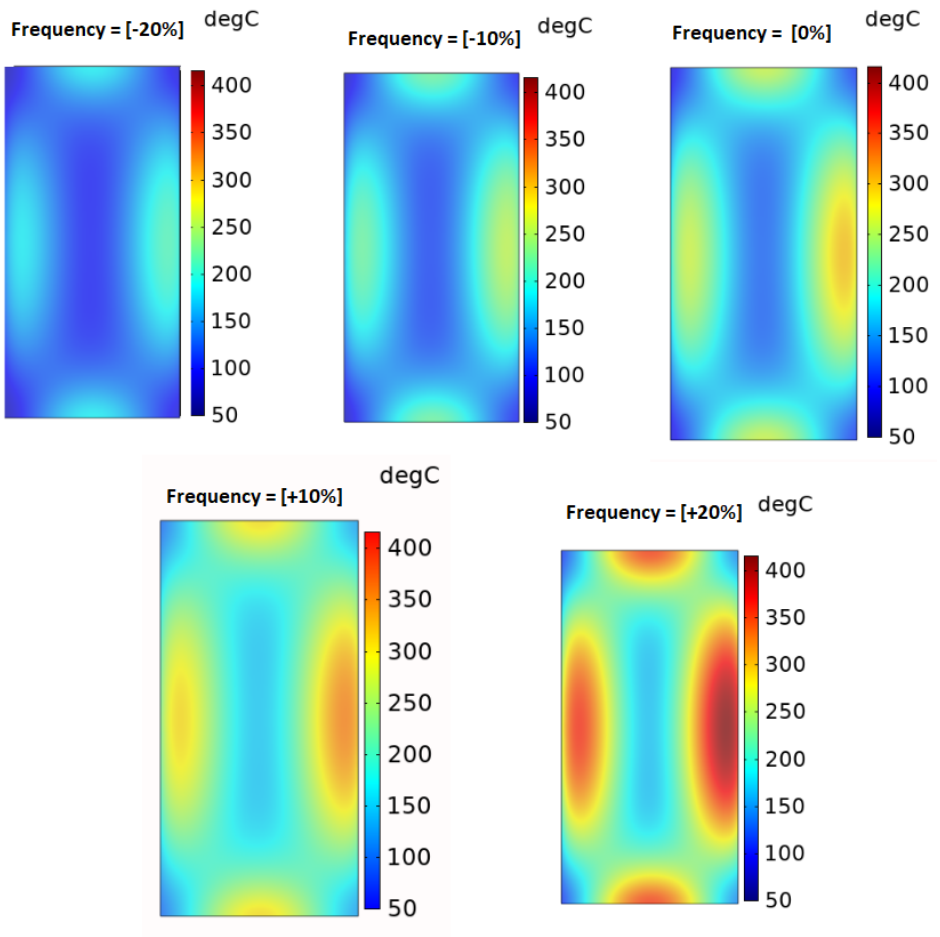

Figure 3.27: Susceptor temperatures for sensitivity analysis for different frequencies

Frequency places important role on both computation and temperature, changing frequency not only affects temperature significantly but also it affects computational cost. As for high frequencies because of small skin-depth there is need for high density mesh element size.

Coupling distance: Figures 3.28 and 3.29 show sensitivity analysis for coupling distance between the coil and susceptor. Deviation of 7% for 10% decrease in coupling distance is observed. Accordingly coupling distance has the least significance among machine parameters in induction heating.

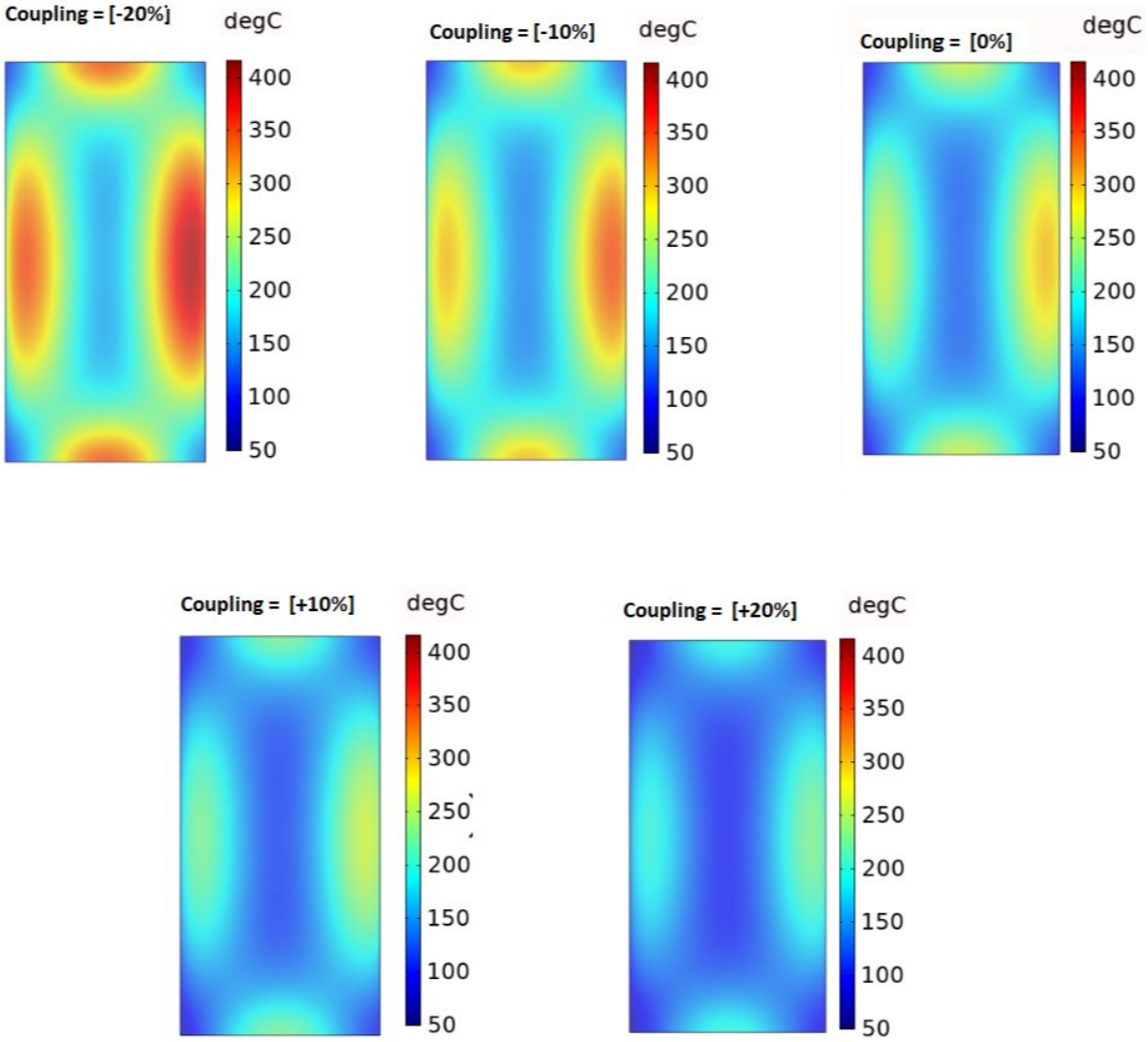

Figure 3.28: Susceptor temperature for sensitivity analysis for different coupling distances

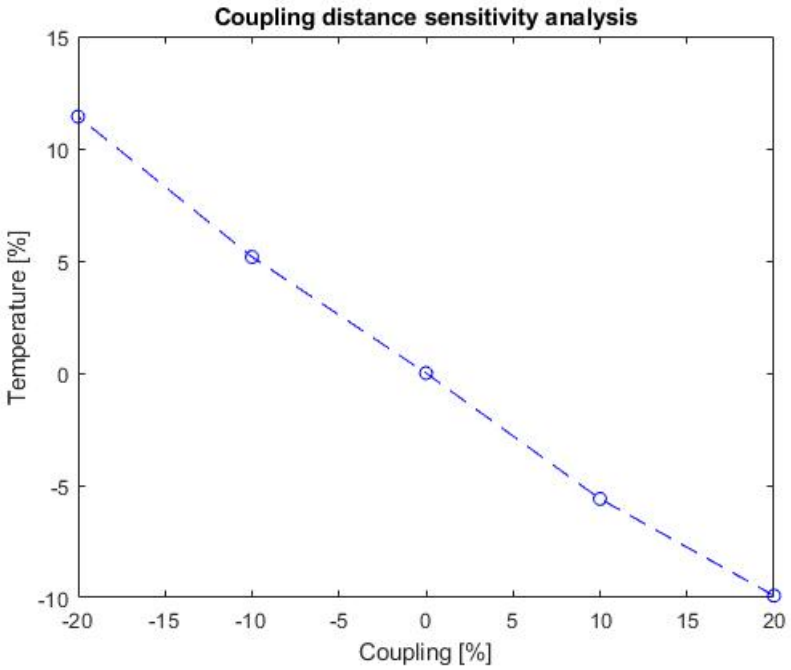

Figure 3.29: Sensitivity analysis for coupling distance

Coil current: Figures 3.30 and 3.31 demonstrate the influence of the coil current on average temperature. Deviation of 9% for 10% increase in coil current can be observed. Accordingly the coil current is also a parameter with high significance for induction heating after frequency.

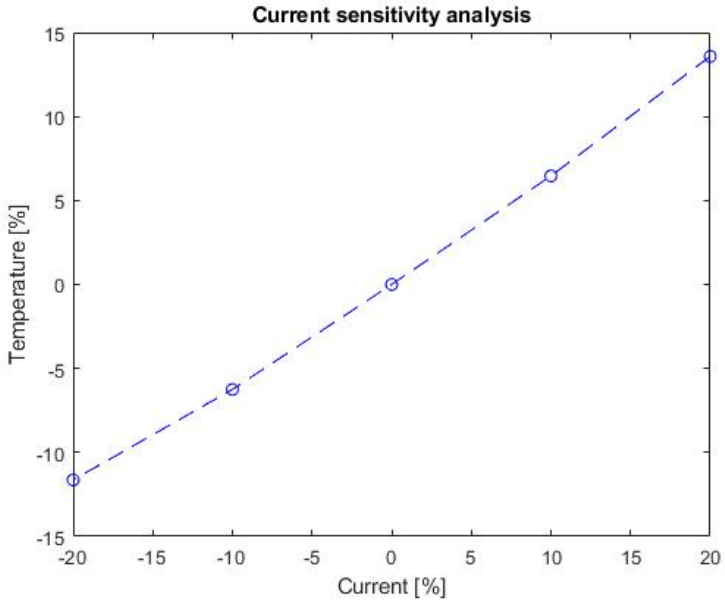

Figure 3.30: Sensitivity analysis for coil current

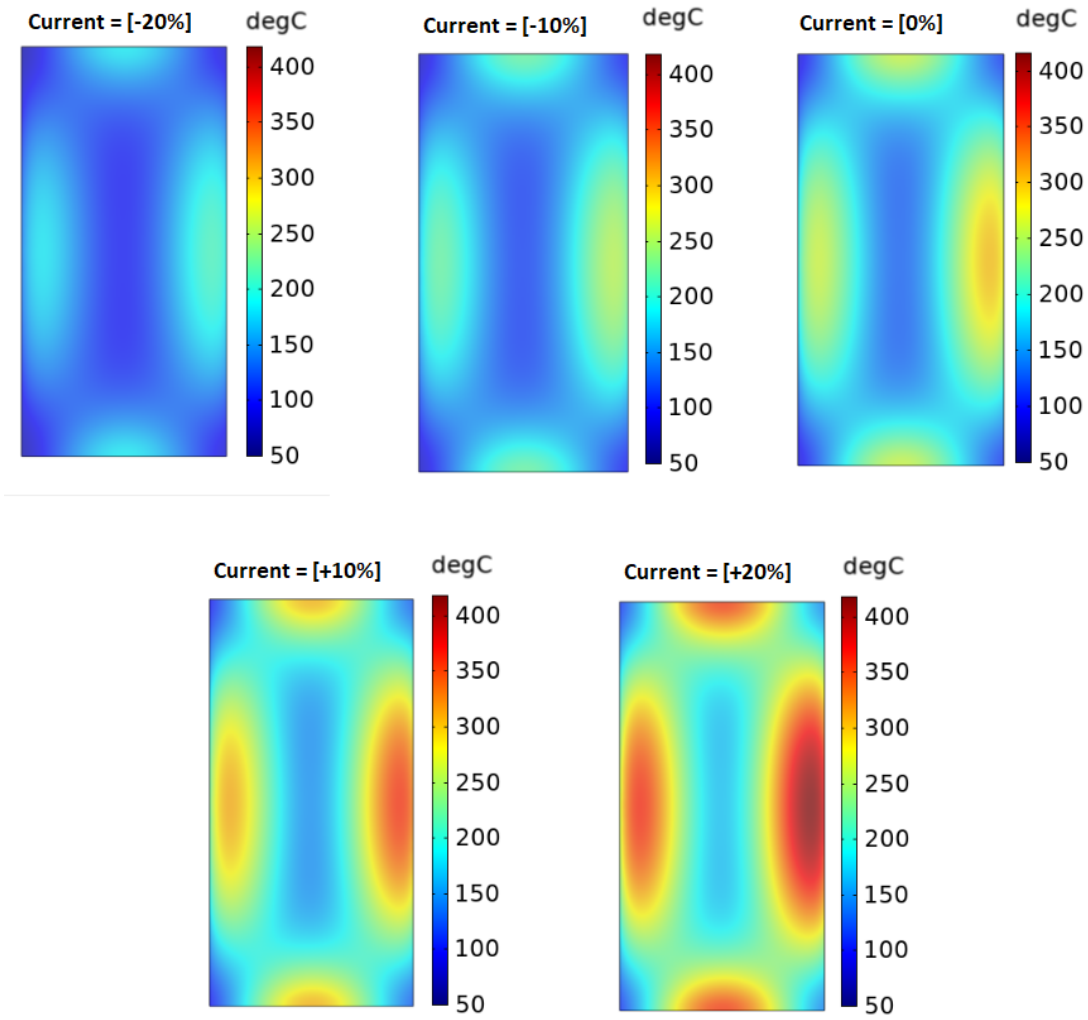

Figure 3.31: Susceptor temperature for sensitivity analysis for different coil currents

Heat capacity & **heat conductivity:** Sensitivity analysis for heat capacity was performed. As Figure 3.32 demonstrates deviation of 0.12% for 10% increase in heat capacity can be observed. Accordingly heat capacity has negligible effect on heat generation process.

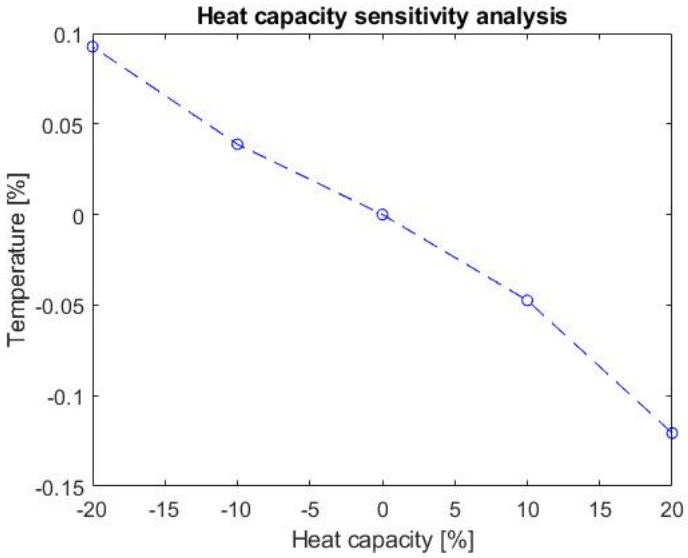

Figure 3.32: Sensitivity analysis for heat capacity

Sensitivity analysis for both in-plane and out of plane heat conductivity was performed. As Figure 3.33 demonstrates deviation of 0.03% for 10% increase in heat conductivity can be observed. Accordingly heat conductivity has negligible effect on heat generation.

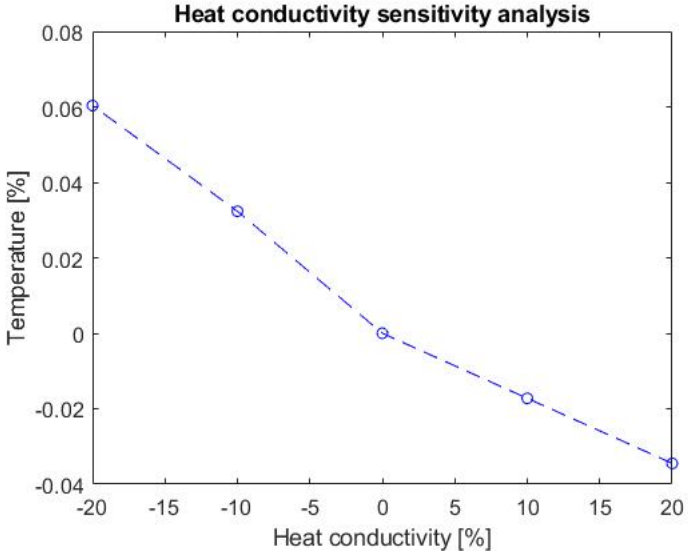

Figure 3.33: Sensitivity analysis for frequency

Electrical conductivity: Sensitivity analysis for electrical conductivity was performed. As Figure 3.34 and 3.35 demonstrate deviation of 3.8% for 10% increase

in electrical conductivity can be observed. Accordingly electrical conductivity has accountable effect on heat generation process.

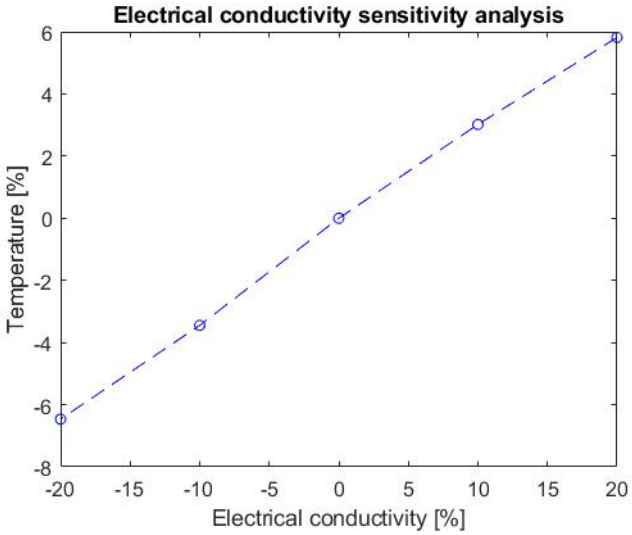

Figure 3.34: Sensitivity analysis for electrical conductivity

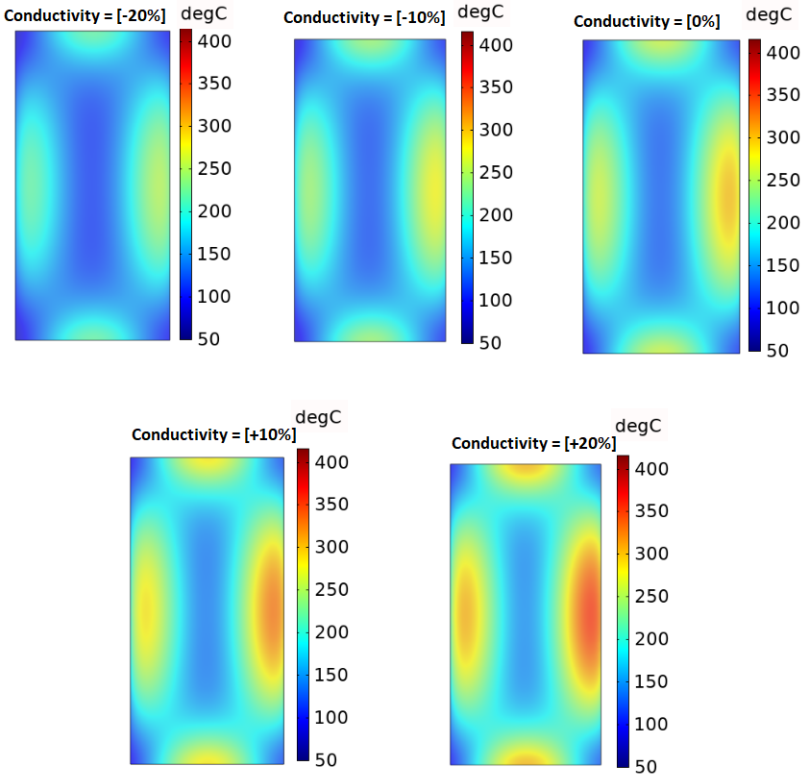

Figure 3.35: Susceptor temperature for sensitivity analysis for different electrical conductivities

4

Experiment

In order to validate results from simulation model experiment for induction welding has been done at thermoplastic composites laboratory at École de technologie supérieure, ÉTS in Montreal, Canada.

4.1 Experiment set-up

Figure 4.1 demonstrates the induction welding machine. Induction welding was performed on samples. Figure 4.2 demonstrates dimensions for samples used in the experiment. Temperature history was measured at the welding interface using K-type thermocouples. The induction welding setup includes an induction heating device (power supply and work head), a pneumatic cylinder to apply pressure, a welding jig, and a temperature acquisition system. The induction heating device is a 10 kW Ambrell Easy Heat machine with a frequency ranging from 150 kHz to 450 kHz and maximum out put of 750 A.

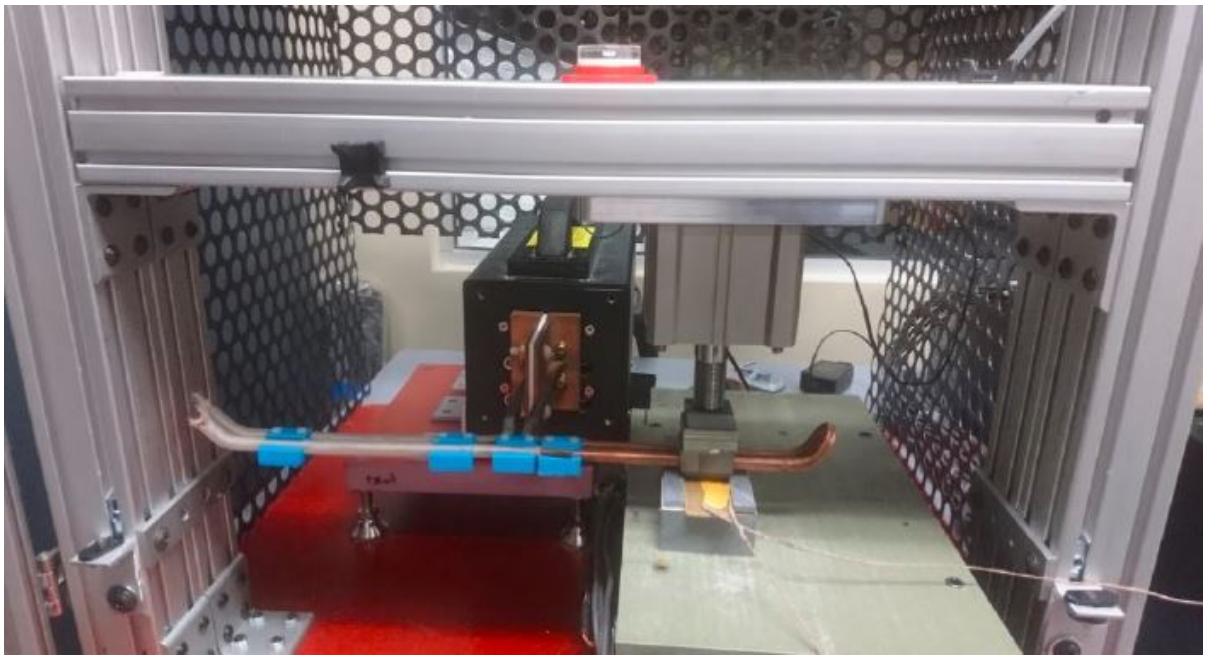

Figure 4.1: Welding set-up

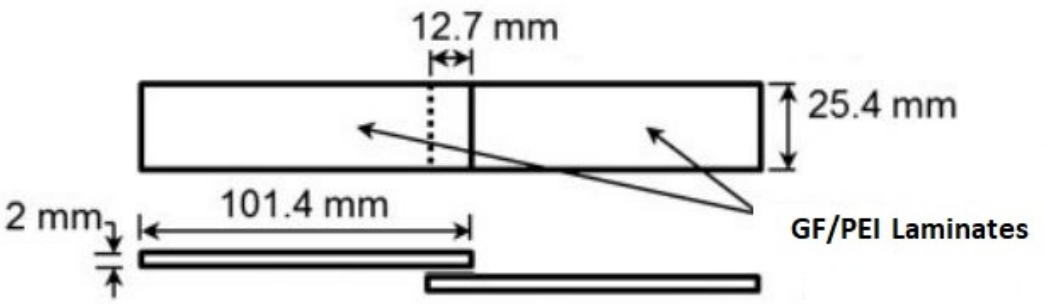

Figure 4.2: Dimensions for sample

4.2 Welding set-up

After cutting laminates according to ASTM1002D, as Figure 4.3 is demonstrating, a layer of neat thin film of PEI is placed on both side of the susceptor at the welding interface. This neat film helps for better squeeze out and removing air bubbles at the weld zone. A thermocouple is placed at the welding interface 3mm of the edge of susceptor as it is shown in Figure 4.4, where edge-effect is present. The position of the thermocouple is shown in the Figure 4.3. Dimensions for the susceptor are 25.4mm by 12.7mm with the thickness of 80μm. The dimensions of neat film PEI are 25.4mm by 12.7mm with the thickness of 100μm.

Figure 4.3: Welding set up

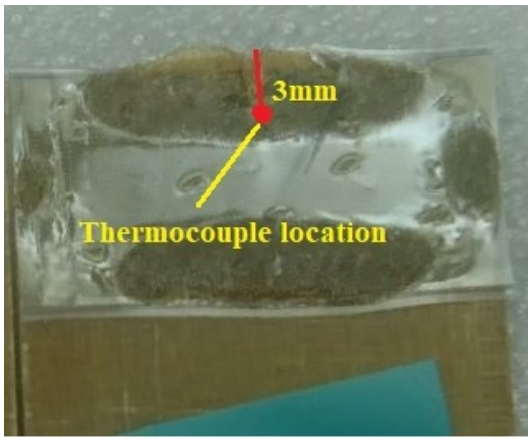

Figure 4.4: Thermocouple location

4.3 Welding parameters

The coil frequency is chosen automatically by the welding machine at 265kHz. So the only parameters to modify are coupling distance and coil current. After multiple tests for identifying the significance of thermal degradation due to edge-effects and temperature gradient, it was decided to set the coupling distance to 5 mm and the current to 471 Ampere. The applied pressure was 0.8MPa for all tests. Welding machine is programmed to cut the power automatically when temperature reaches to 350 degrees. The reason for choosing auto shut down is due to safety.

Weldings with two different output currents are presented below, Figure 4.5 shows welding with 550 Ampere current in the coil. Figure 4.6 shows welding interface with 471 Ampere current in the coil.

Figure 4.5: Welding with 550 A

As Figure 4.5 shows, for the current of 550 Ampere, there is a region where material degradation is observed due to high temperature gradient. The reason for such a high temperature gradient at the welding interface is due to high heat capacity

of PEI matrix as well as low heat conductivity of the glass fiber and PEI matrix. Such a low heat conductivity results in heat to be trapped in areas where we have edge-effects and results in high temperature gradient. As it was also discussed for Figure 3.23, on the side where there is ceramic support thermal degradation has not occurred while for the upper side heat traps in the edge-effect zone and it resulted in thermal degradation. Observation from welding with 471 Ampere shows most materials at the welding interface are not melted. These experiments show GF/PEI is such challenging material to weld and reveals the need for designing a susceptor with improved thermal and electrical conductivities.This will be the future work.

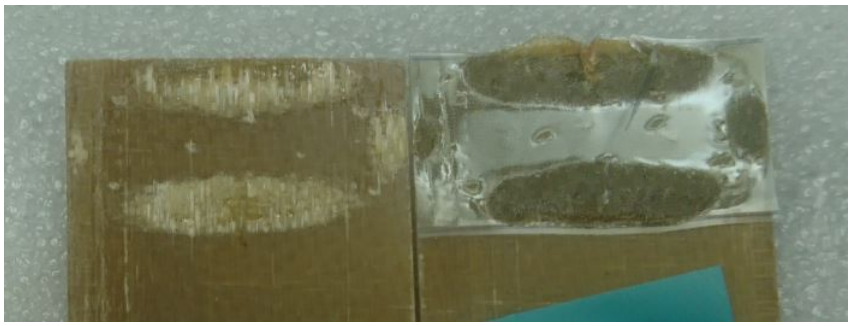

Figure 4.6: Welding with 471 Ampere

Temperature history: Figure 4.7 temperature history captured by a termocouple 3mm off the edge of susceptor.

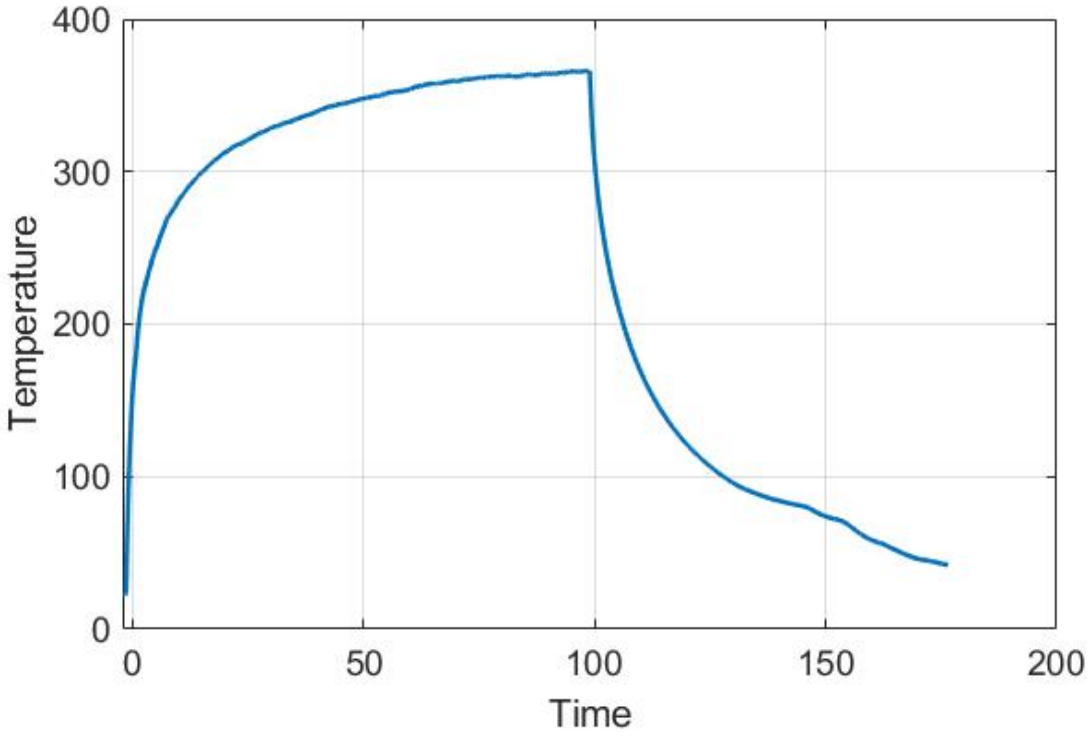

Figure 4.7: Welding process temperature history

4.4 Idea for conductive cooling at the edge-effect

As it can be observed in Figure 4.5, in welding with 550 Ampere thermal degradation occurs. Thermal degradation affects mechanical performance of the weld and results in weak joints. There have been different methods to tackle this issue. For example Moser et. al [21] has suggested forced convection for cooling the surface in welding carbon fiber thermoplastics for susceptorless induction welding. However this method can not be used as in our study the heat is concentrated at the welding interface. As Figure 4.8 shows there is a high temperature gradient at the right side of the welding zone due to edge-effect, while for the left side a tiny contact between susceptor and the ceramic support of the welding jig has reduced the temperature gradient and eliminated the thermal degradation.

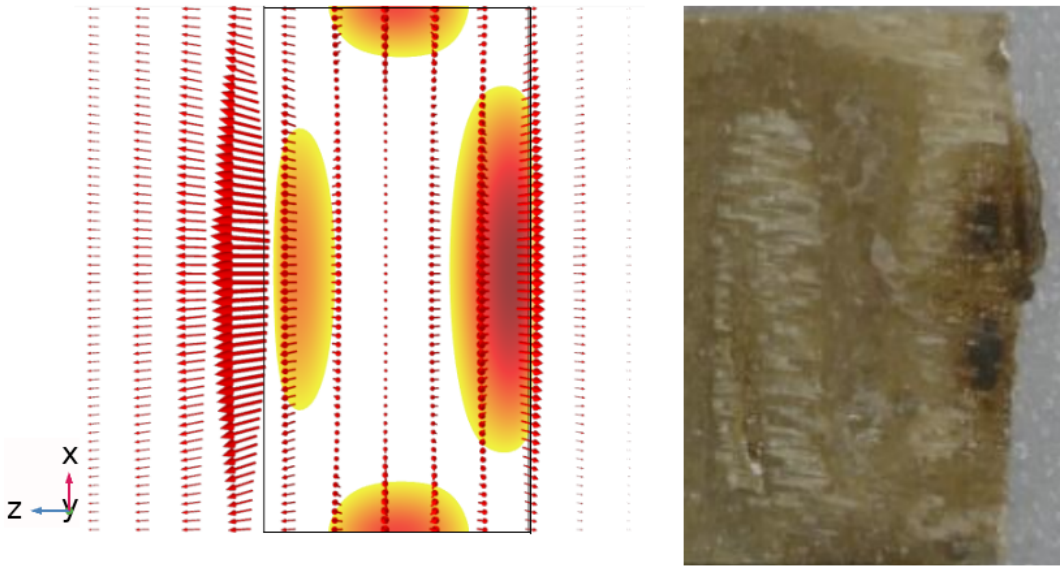

Figure 4.8: Bypassing heat at the welding interface (top view)

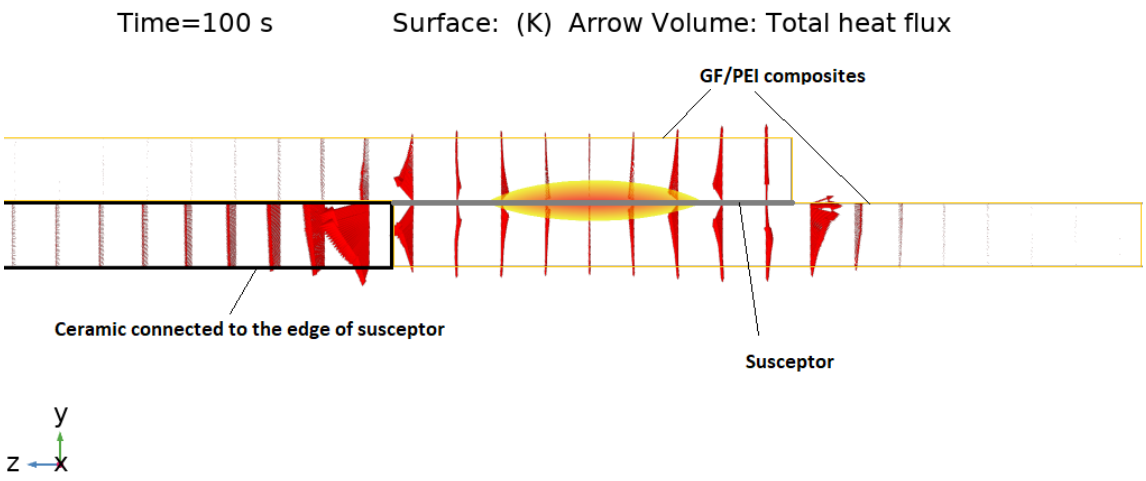

Figure 4.9: Bypassing heat at the welding interface (side view)

This is due to the fact that the ceramic has higher thermal conductivity compared to GF/PEI, so it acts as a heat sink. Figure 4.9 shows the side view of the coupons and ceramics. As it can be observed there is a significantly larger heat flow on the left side in Figure 4.9 and that is why there is no thermal degradation in that part.

Temperature history was measured on both side of susceptor at locations with 2mm off the edge as it is shown in Figure 4.10. As the plot is showing after $t = 27$ seconds onward, for heating with the frequency of 265 kHz, the current of 550 Ampere and coupling distance of 5.5mm, temperature in the region with conductive cooling is noticeably less than the opposite side. Such a temperature difference seems to be sufficient to prevent thermal degradation on the left side.

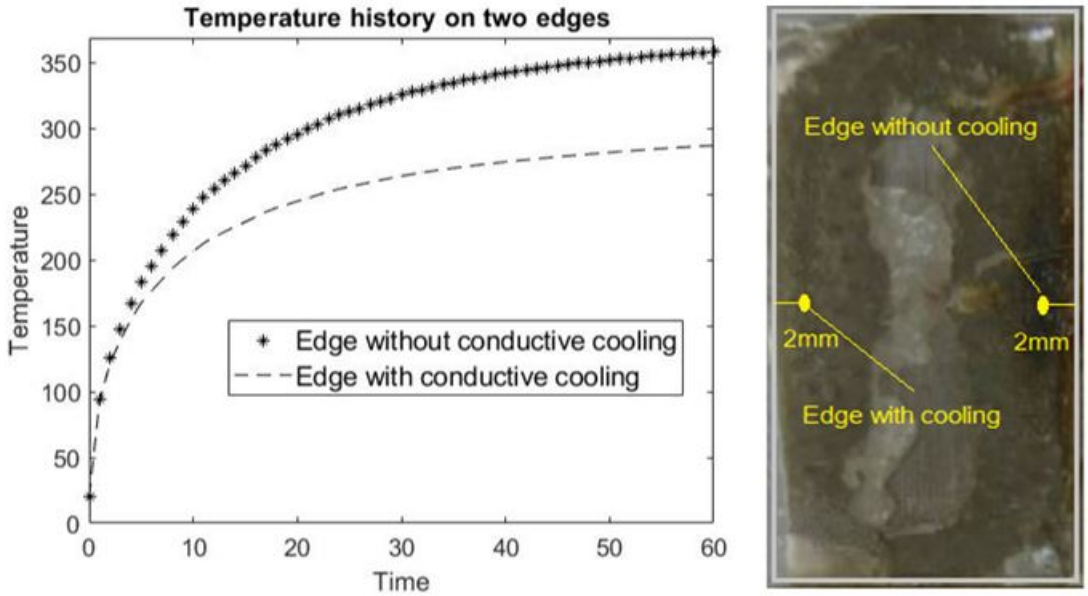

Figure 4.10: Comparison between temperature history on both side

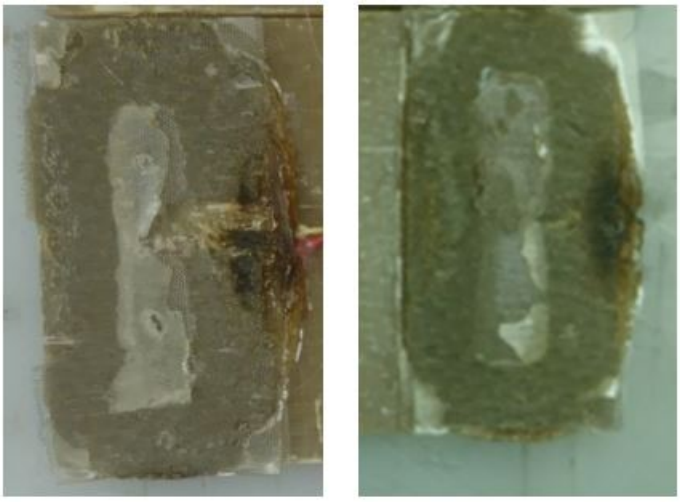

Figure 4.11: Two more samples welded by 550 Ampere with conductive cooling

Conductive cooling or bypassing heat could be a simple and cheap solution to control the excessive heat on the edge of susceptor due to edge-effect. Specially when dealing with material such as GF/PEI in which behaves as a heat insulator due to low heat conductivity. These properties of GF/PEI makes it such a challenging material to work with.

Figure 4.12 demonstrates welding carbon fiber-polyphenylene sulfide (CF/PPS) compared to GF/PEI. As it is shown there is non melted materials at the welding interface due to low in plane heat conductivity of GF/PEI. However looking at CF/PPS there is no unmelted material at the welding interface. This is due to high heat conductivity and electrical conductivity of the carbon fibers in which not only contribute in heat generation but also improve in plane heat conductivity at the welding interface.

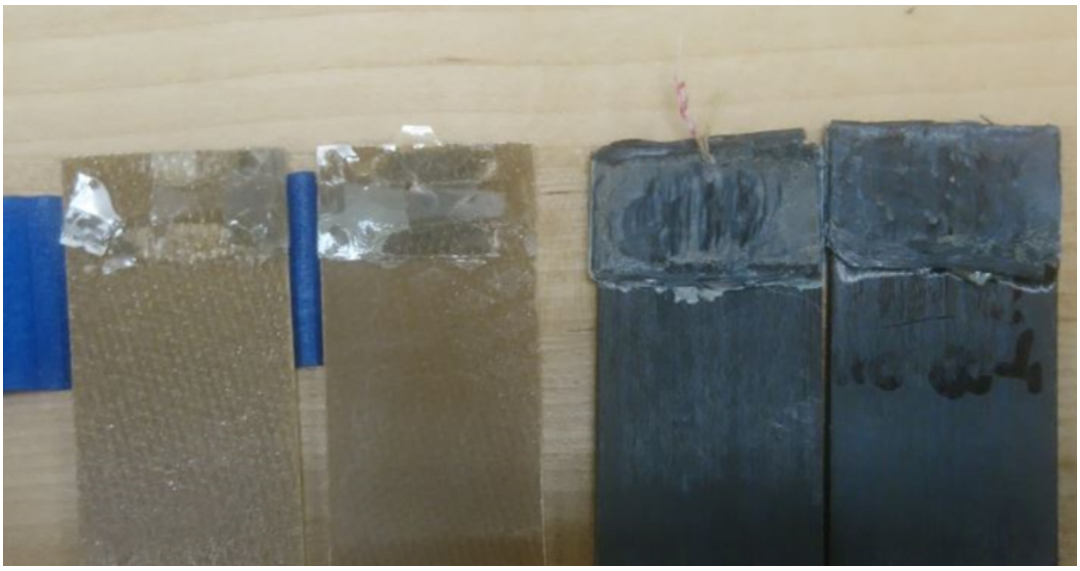

Figure 4.12: Comparison between "Carbon Fiber-Polyphenylene sulfide" and "Glass Fiber polyetherimide"

5
Validation

5.1 Simulation model validation

Figure 5.1 demonstrates temperature distribution history during 100s of induction heating process at the welding interface. The welding parameters for experiment and simulation model is shown in Table 5.1.

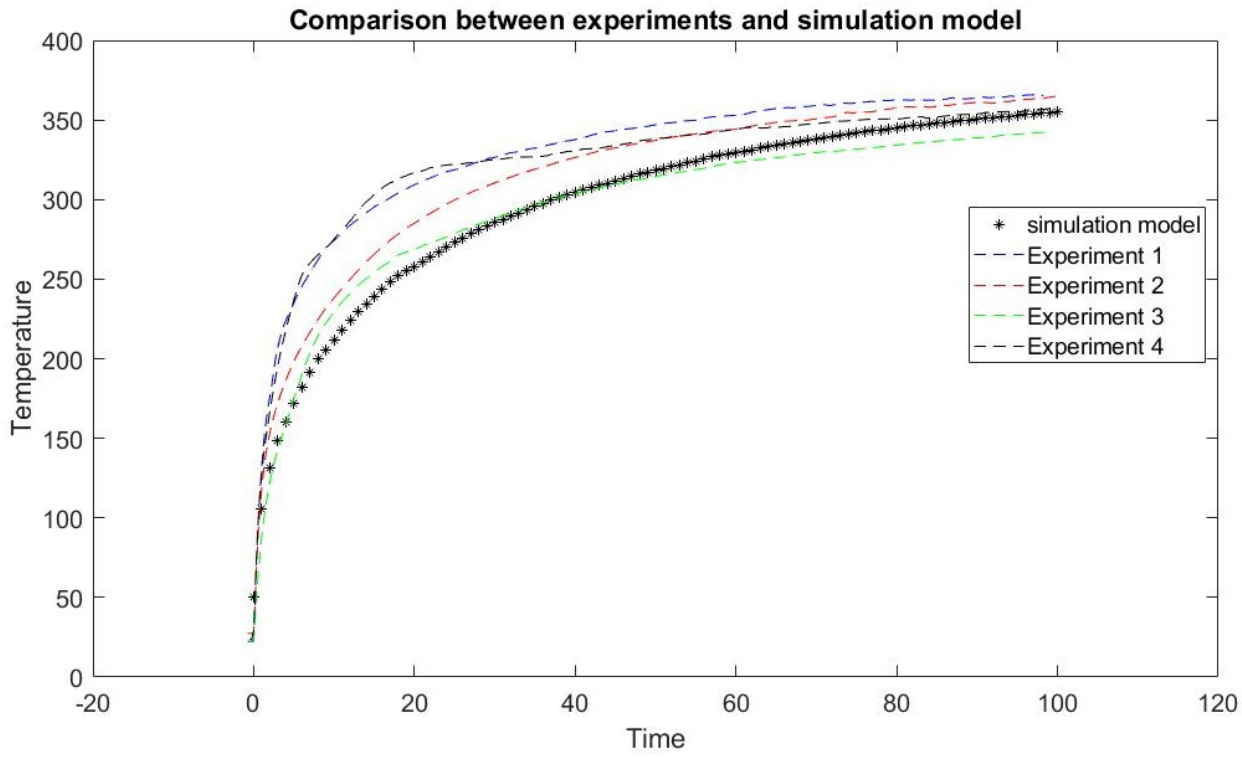

Figure 5.1: Comparison between experimental results and simulation model

Reference parameters	Unit	Value
Coupling distance	mm	5
Coil current	Ampere	471
Coil frequency	kHz	265

Table 5.1: Machine parameters

5.2 Error identification

When it comes to conducting experiments for validating the simulation model, it is important to know what makes the simulation model different from experiment. Also it is important to understand which condition is idealized in the simulation model compared to experiment. Below the two most important factors affecting our experiment have been discussed.

5.2.1 Thermocouple

Different factors can affect the difference between simulation and experiment results. For this experiment the sensor used for measuring the temperature was K-type thermocouple. Since thermocouples are electrically conductive there is induced current in the thermocouple which appears as error. This error was measured by exposing the thermocouple to the coil with the same welding parameters and the measured error is about 30 degrees which was added to the final result of simulation. So one of the reasons for having higher rate of raising temperature in the experiment is due to induced current in the thermocouple.

Figure 5.2 demonstrates the induced current which appears as error in the thermocouple. The effect of induced current in thermocouple on final result of simulation with and without correction are demonstrated in Figure 5.3.

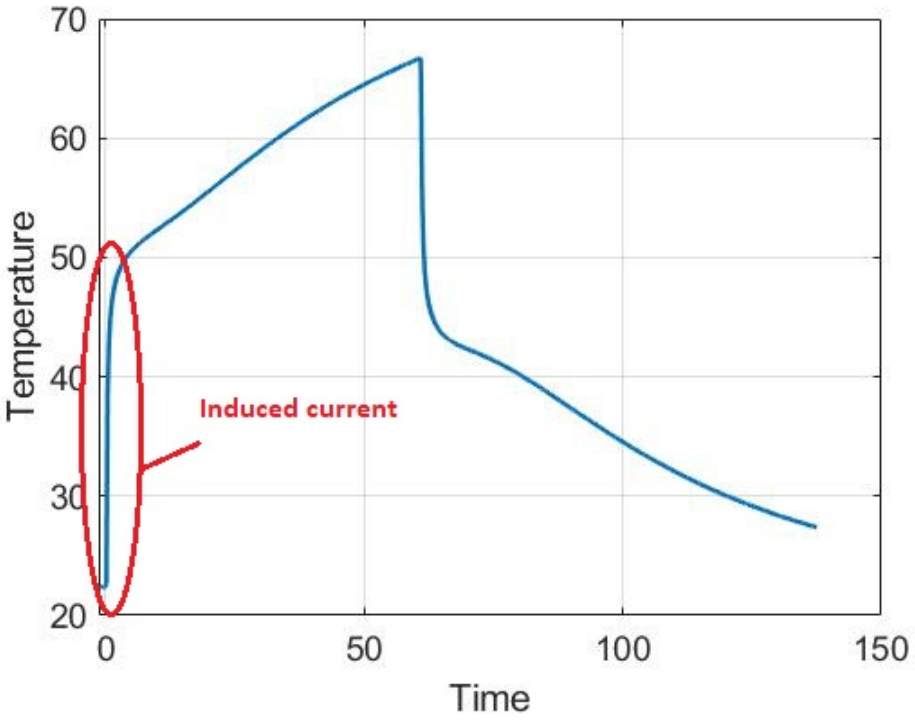

Figure 5.2: Induced current in thermocouple

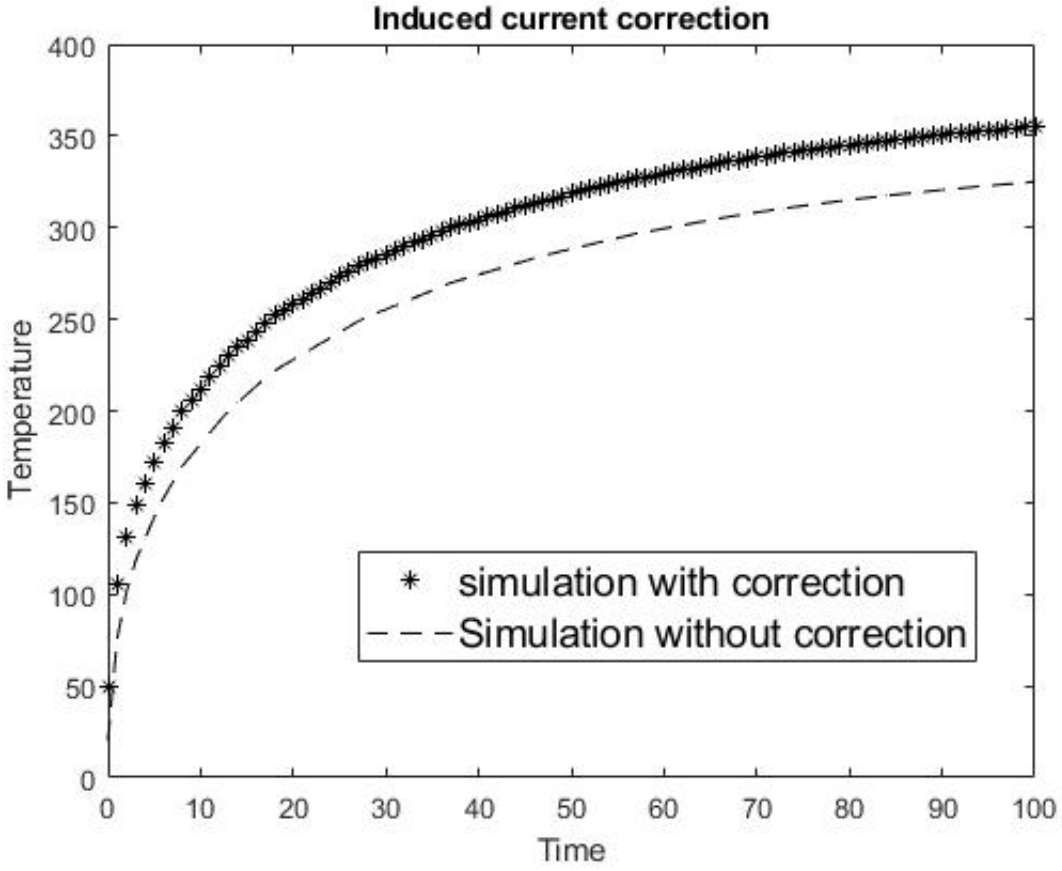

Figure 5.3: Comparison between simulation result with and without correction of induced current

5.2.2 Contact and surface smoothness

The second most important factor resulting in error is the contact between components at the welding jig. The simulation model all surfaces are perfectly smooth and the contact between all components is assumed flawless and perfect. This results in an idealized heat conduction between different components at the welding jig in the simulation model. Such an idealized heat conduction between components results in lower heating rate in the simulation model compared to experiments. Grooves and lack of perfect contact in experiment affect heat conductivity and heat remains trapped which results in higher rate of heating.

One way to demonstrate this is by considering non smooth contacts equivalent to lower heat conductivity and assume higher heat conductivity equivalent to perfect contact. Accordingly, Figure 5.4 shows how 40% increase and 40% decrease in heat conductivity of ceramic components of the welding jig can affect the mean temperature of the susceptor. As it can be observed the maximum 4.5% deviation of mean temperature of susceptor is observed for 40% decrease in heat conductivity of the ceramic support. The plot in Figure 5.4 shows that when the heat conductivity of ceramic support is reduced the heat is trapped in the susceptor and higher mean

temperature of susceptor is observed.

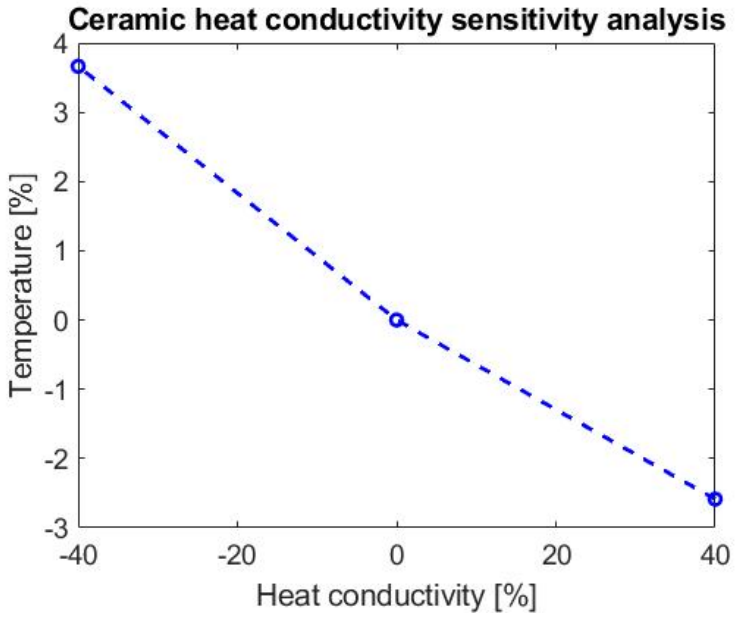

Figure 5.4: Heat conductivity of ceramic affecting mean temperature at welding interface

Such a deviation by changing heat conductivity shows that smoothness of the contact surface between components of the welding jig plays an important role in the heat transfer. Considering these errors, also by comparing results from experiment and simulation model in Figure 5.1, the simulation model shows sufficient accurate prediction of temperature history during welding process.

6
Conclusion

Validation of simulation result with experiment showed acceptable accuracy. The model proposed by Holms et. al [32] for homogenisation of thermal conductivity of GF/PEI laminate was used. Also, the model for homogenization of thermal and electrical conductivity of susceptor according to Writz et. al [31] provided estimation of in plane and out of plane material properties.

However welding GF/PEI proved to be very challenging. Due to low heat conductivity of the PEI polymer and glass fibers high temperature gradients occur at the welding interface. Edge effect on susceptor results in thermal degradation and low conductivity of materials result in unmelted polymer at the welding interface. A simple solution was suggested to prevent thermal degradation by bypassing the heat at the edge effect zone. However, in order to gain a homogeneous heat distribution at the welding interface there is a need for designing susceptor where heat and electrical conductivities are optimised in a 3D network. Since none of the softwares currently available provide simulation for intimate contact and consolidation, the focus of this thesis was limited to modeling induction heating for induction welding process.

Results from sensitivity analysis showed that machine parameters such as coupling distance, current and frequency have the highest effect on the heat generation process. In terms of material properties, heat capacity and thermal conductivity have negligible effect on heat generation process while electrical conductivity has noticeable effect on heat generation in the susceptor.

6.1 Future work

For the future work as a PhD student the focus will be addressing issues observed during experiments. The main issues in induction welding GF/PEI using conventional metal mesh susceptor are listed as below

- Spots with high temperature gradients due to edge effect.
- Unmelted polymer at the welding interface because of low heat conductivity of PEI polymer.
- Low heating rate due to low electrical conductivity of the metal mesh susceptor.

Issues mentioned above can affect mechanical performance of the weld. Recommended solution to improve weld quality lays in preventing high temperature gradient and improving electrical and thermal conductivity in the susceptor. This can not be done using conventional metal mesh susceptor. In order to generate homogeneous heat at the welding interface, it is required to design a susceptor by distributing electrically conductive nano particles such as graphene, nano wires and etc. This distribution must first counter act the pattern of magnetic field on the susceptor to avoid edge effect, secondly it should provide with fast heating rate and improved heat conductivity at the welding interface to prevent unmelted regions.

Bibliography

[1] Benatar, A.; Gutowski, T. G.: *Methods for Fusion Bonding Thermoplastic Composites.* SAMPE Quarterly 18 (1986), Issue 1, 35-42.

[2] Grewell, D. A.; Benatar, A.; Park, J. B.: *Plastics and Composites Welding Handbook.* Munich: Hanser, 2003.

[3] Bruce K. Fink, Shridhar Yarlagadda, and John W. Gillespie Jr. *Design of a Resistive Susceptor for Uniform Heating During Induction Bonding of Composites.* Army research laboratory, 2000.

[4] Patrice Gouin O'Shaughnessey, Martine Dube´ and Irene Fernandez Villegas. *Modeling and experimental investigation of induction welding of thermoplastic composites and comparison with other welding processes.* SAGE 2015.

[5] Jorge D´ıaz, Luis Rubio. *Developments to manufacture structural aeronautical parts in carbon fibre reinforced thermoplastic materials.* ELSEVIER, Spain 2003.

[6] Imad Zammar1, M. Saiful Huq, Iraj Mantegh, Ali Yousefpour and Mojtaba Ahmadi1 *A three-dimensional transient model for heat transfer in thermoplastic composites during continuous resistance welding.* AMPCS 2017

[7] Benoit Vieille, Jérémie Aucher, Lakhdar Taleb, *Woven ply thermoplastic laminates under severe conditions: Notched laminates and bolted joints.* Composites Part B, 2011

[8] C.Ageorges and L.Ye. *Fusion bonding of polymer composites from basic mechanism to process optimisation.* 2002, Springer-Verlag London Ltd.

[9] Yousefpour, A.Hojjati, M.Immarigeon, *Fusion Bonding/Welding of Thermoplastic Composites.* Journal of Thermoplastic Composite Materials 17 (2004), Issue 4, 303-341.

[10] Yarlagadda, S.; Kim, H. J.; Gillespie, J. W., Jr.; Shevchenko, N. B.; Fink, B. K. *A Study on the Induction Heating of Conductive Fiber Reinforced Composites. Journal of Composite Materials* 36 (2002), Issue 4, 401-421.

[11] Xiao, X. R.; Hoa, S. V.; Street, K. N.: *Processing and Modeling of Resistance Welding of APC-2 Composite.* Journal of Composite Materials 26 (1992), Issue 7 (1992), 1031-1049.

[12] Wool, R. P.; O'Connor, K. M.: *Time Dependence of Crack Healing.* Journal of Polymer Science: Polymer Letters Edition 20 (1982), Issue 1, 7-16.

[13] Ageorges C, Ye L, Mai Y-W, Hou M. *Characteristics of resistance welding of lap shear coupons. Part III: crystallinity.* Composites Part A 1998;29A:921±32.

[14] Unger WJ, Hansen JS. *The effect of cooling rate and annealing on residual stress development in graphite fibre reinforced PEEK laminates.* Journal of Composite Material 1993;27:108±37.

[15] Tatiana Oršulova 1, Peter Palček 1, Jozef Kudelcik. *Effect of plastic deformation on the magnetic properties of selected austenitic stainless steels.* Production engineering 2013.

[16] *Haimbaugh RE. Practical induction heat treating.* ASM International 2001.

[17] T.J. Ahmed, D. Stavrov, H.E.N. Bersee , A. Beukers. *Induction welding of thermoplastic composites—an overview.* Journal of applied science and manufacturing, 2005.

[18] Rudolf R, Mitschang P, Neitzel M. *Welding of high-performance thermoplastic composites.* Polym Polym Comp 1999;7:309–15.

[19] Yarlagadda S, Fink BK, Gillespie Jr JW. *Resistive susceptor design for uniform heating during induction bonding of composites.* J Thermoplast Comp Mater 1998;11:321–37.

[20] Selvaged *susceptor for thermoplastic welding by induction heating,* April 1996. Patent no: US5508496.

[21] Lars Moser. *Experimental Analysis and Modeling of Susceptorless Induction Welding of High Performance Thermoplastic Polymer Composites.* Institut für Verbundwerkstoffe GmbH - Kaiserslautern, 2012.

[22] Rudolf R, Mitschang P, Neitzel M. Induction heating of continuous carbon-fibre-reinforced thermoplastics. Comp Part A: Appl Sci Manufact 2000;31:1191–202.

[23] C.M Worrall, R.J. Wise *Novel Induction heating technique for joining of carbon fiber composites.* European conference on composites material, 2014.

[24] R.D Farahani, M. Dube *Novel Heating Elements for induction welding of carbon fiber/polypheylene Sulfide Thermoplastic Composites.* Advanced Engineering Materials 2017.

[25] Danilo Mattheß, Dirk Landgrebe and Welf-Guntram Drossel. *Inductive heating of glass fibre-reinforced thermoplastics using fibre- and wire-shaped stainless steel susceptors.* Journal of Thermoplastic Composite, 2017.

[26] David J. Griffiths *Introduction to electrodynamics* PEARSON, 2013.

[27] Thomas A. Lipo, *Electromagnetic Modeling power electronic converters*, Springer, 1989.

[28] Valery Rudnev, Don Loveless, Raymond L. Cook *The handbook of inductive heating.* CRC press, 2017.

[29] COMCOL multiphysics 5.4 AC/DC manual. 2018

[30] J. H. Lienhard: '*heat transfer textbook*, 2013, Cambridge, MA, Courier Corporation

[31] Jun Xu and Richard A. Wirtz. *In-Plane effective thermal Conductivity of plain-weave screen laminates.* IEEE 2002.

[32] Scott T. Holms, John W. Gillespie. *Thermal Analysis for Resistance Welding of Large-Scale Thermoplastic Composite Joints.*Journal of reinforced plastics and composites, 1993.

[33] C. Ageorgesa, L. Ye, M. Hou *Advances in fusion bonding techniques for joining thermoplastic matrix composites: a review.* Applied science and manufacturing, ELSEVIER, 2001.

[34] Jun Xu and Richard A. Wirtz. *In-Plane Effective Thermal Conductivity of Plain-Weave Screen Laminates.* IEEE 2002.

[35] Edith Talbot. *Manufacturing process modeling of thermoplastic composite resistance welding*. 2005. McGill University, Montreal
[36] Tencate product datasheet, 2016.